UNIVERSIDADE D
COIMBRA

Gabriela Sampaio Ribeiro

UNRAVELING THE INTERPLAY BETWEEN FIBROBLASTS AND OSTEOSARCOMA CELLS DURING LUNG METASTASIS FORMATION

Dissertação no âmbito do Mestrado em Investigação Biomédica orientada pela Doutora Célia Maria Freitas Gomes e pela Mestre Sara Filipa Fernandes de Almeida e apresentada à Faculdade de Medicina da Universidade de Coimbra.

Outubro de 2021

UNIVERSIDADE D
COIMBRA

Gabriela Sampaio Ribeiro

UNRAVELING THE INTERPLAY BETWEEN FIBROBLASTS AND OSTEOSARCOMA CELLS DURING LUNG METASTASIS FORMATION

Dissertação no âmbito do Mestrado em Investigação Biomédica orientada pela Doutora Célia Maria Freitas Gomes e pela Mestre Sara Filipa Fernandes de Almeida e apresentada à Faculdade de Medicina da Universidade de Coimbra.

Outubro de 2021

This work was funded by the Portuguese Foundation for Science and Technology (FCT) through the project PTDC/BTM-SAL/4451/2020, Strategic Project UIDB/04539/2020 and UIDP/04539/2020 (CIBB) and by Liga Portuguesa contra o Cancro/Lions Portugal.

Agradecimentos

Aqui findam dois anos de grande aprendizagem e evolução, tanto profissional como pessoal. Foi um percurso intenso, mas nunca me senti tão realizada como neste último ano, onde realmente fiz o que sempre quis, investigação. Conheci pessoas incríveis, verdadeiras mentes brilhantes, que me abriram as portas da ciência, do conhecimento e do desenvolvimento. Pessoas a quem eu agradeço todo o apoio e dedicação.

Primeiramente, agradeço às pessoas mais importantes deste percurso, às minhas orientadoras. À Doutora Célia Gomes, uma investigadora brilhante que me ajudou durante todo este ano, incentivou e me transmitiu todo e mais algum conhecimento. Mesmo no final de um longo dia de trabalho, estava sempre disponível para tirar dúvidas ou planear uma experiência, apelando sempre pelo meu sentido crítico, e sempre me ajudando a chegar cada vez mais longe. À Sara Almeida, uma química que me ensinou tanto sobre biologia celular. Tenho muito orgulho em dizer que fui a primeira aluna a ser orientada por esta investigadora, que de certeza, ainda dará muitas cartas na ciência. A ela agradeço por toda a paciência, tempo e dedicação para me ensinar tudo o que precisava de maneira a ser independente num laboratório. Sempre a correr, não fosse ela aluna de doutoramento, mas sempre preocupada se eu precisava de alguma coisa. O meu muito obrigada às duas!

Agradeço também às minhas colegas do laboratório. À Liliana, que também sempre me apoiou e tirou qualquer dúvida que tivesse, estando sempre disponível para me ajudar. A quem eu agradeço por todos os conselhos e tempo dedicado. À Ana Filipa, que foi a minha colega, também aluna de mestrado, em que partilhámos e vivemos dia a dia durante este ano. Também agradeço à Margarida e à Diana pelas conversas descontraídas e conselhos.

Agradeço ao Doutor Henrique Girão, o meu coordenador de mestrado, sem o qual este percurso não teria acontecido. O MIB foi definitivamente a melhor escolha

académica que fiz até agora. Um mestrado que me deu as bases que necessitava e que me permite hoje dizer que sou uma investigadora biomédica. Obrigada por todos os conselhos e conhecimentos transmitidos.

Agradeço também ao instituto que me acolheu para a realização deste projeto, ao iCBR e à Faculdade de Medicina da Universidade de Coimbra.

Quero agradecer também a todas as pessoas que se cruzaram comigo neste percurso e me deram dicas e sugestões para melhorar as experiências aqui apresentadas nesta dissertação.

Por fim, quero agradecer a pessoas muito importantes que sempre me apoiaram durante todas as decisões tomadas e em todo o meu percurso académico e de vida. À minha família, que me viram batalhar durante este ano, a chegar tarde a casa e que se habituaram à minha ausência em alguns fins de semana. Espero que me continuem a acompanhar e a apoiar neste caminho, que como sabem não acaba aqui. Dedico especialmente esta tese à minha mãe, que sempre me ouviu, tanto em momentos de pura felicidade como em momentos menos bons. Mesmo sem formação científica, já sabe o que é um western blot, um PCR ou até culturas primárias. Esteve sempre do meu lado e eu sempre a apoiarei.

Agradeço também ao Daniel, que sempre me ouviu e apoiou e sabe o quão especial ele é para mim. Agradeço também a amigos que já são família, aos quais este ano nos afastou, mas sei que continuamos sempre com a ótima relação que construímos. À Bea, à Jessica, ao Carlos, à Inês e ao Fidalgo uns doidos que conheci na licenciatura que espero e vou fazer com que me acompanhem para o resto da vida.

Bom, o mestrado já está! Agora que venha o próximo desafio!

Resumo

Introdução: *O osteossarcoma (OS) é um tumor primário maligno que usualmente metastiza para o pulmão. Evidências crescentes sugerem que o tumor primário promove alterações fenotípicas nos fibroblastos pulmonares residentes, formando um nicho pré-metastático que favorece a colonização e desenvolvimento de metástases pulmonares. Posto isto, avaliámos a modulação do microambiente pulmonar e os efeitos recíprocos dos fibroblastos ativados sobre as células tumorais antes da colonização do pulmão.*

Materiais e métodos: *Os pulmões foram recolhidos de murganhos não tratados, tratados com o secretoma das células 143B e de murganhos que possuíam um tumor primário subcutâneo. A modulação das proteínas da matriz extracelular (ECM), colagénio I/III e fibronectina foram avaliadas por imunohistoquímica e por western blot. Os fibroblastos pulmonares foram isolados a partir das três diferentes condições e avaliada a expressão de marcadores de ativação (α-SMA, vimentina e fibronectina) por imunocitoquímica e western blot. A capacidade de migração dos fibroblastos pulmonares também foi avaliada por um ensaio de scratch. A expressão de citocinas inflamatórias foi avaliada por qRT-PCR tanto no tecido como nos fibroblastos pulmonares. Depois desta caracterização, as células 143B foram expostas ao secretoma dos fibroblastos normais (NFs), e dos fibroblastos ativados derivados de murganhos tratados com o secretoma das células 143B ($NAFs^{SCR}$) e derivados de animais com um tumor primário ($NAFs^{SCT}$) em diferentes tempos de incubação. A quimiosensibilidade destas células à doxorubicina foi avaliada utilizando um ensaio colorimétrico com resazurina, assim como, características estaminais analisadas por um ensaio de formação de esferas e a expressão de genes de pluripotência e genes alvo da via de sinalização Wnt por qRT-PCR. A indução do estado de dormência foi avaliada por western blot. A adesão das células tumorais à fibronectina foi analisada na presença e na ausência de um anticorpo neutralizador da integrina β1.*

Resultados: *O tecido pulmonar recolhido dos dois modelos animais tratados mostrou um aumento na deposição de fibras de reticulina (colagénio I/III) e fibronectina, e os fibroblastos pulmonares expressaram α-SMA, vimentina e fibronectina, bem como, um aumento significativo de mediadores inflamatórios, sugerindo um estado de ativação.*

As células 143B tornaram-se mais resistentes à doxorubicina, após serem expostas ao secretoma das NAFs^{SCR} e NAFs^{SCT}, e adquirem propriedades estaminais, nomeadamente uma elevada expressão de SOX2 e KLF4, bem como, um aumento na eficiência de formação de esferas e no seu diâmetro. Às 24h de incubação, as células 143B entraram num estado de dormência, mostrado pela elevada expressão de p-p38 e diminuta expressão da pERK, representado por um rácio que muda progressivamente para o seu inverso, promovendo um fenótipo proliferativo. O secretoma das NAFs^{SCR} e NAFs^{SCT} também estimula a adesão das células tumorais à fibronectina, sendo esta ligação mediada pela integrina β1.

Conclusões: *As células 143B, através da secreção de biomoléculas, induzem alterações no parênquima pulmonar e promovem a ativação dos fibroblastos, que têm efeitos recíprocos nas células tumorais, favorecendo a sua resistência à quimioterapia, entrada num estado de dormência antes de iniciarem a sua proliferação e aumentam as suas propriedades de adesão. Estes resultados evidenciam a interação mútua entre os fibroblastos e as células tumorais antes do início da colonização do pulmão. Adicionalmente, alguns destes mecanismos mediados pelos fibroblastos podem representar potenciais alvos para prevenir a formação de metástases pulmonares.*

Palavras-Chave: *Osteossarcoma, metástase pulmonar, nicho pré-metastático, fibroblastos, secretoma.*

Abstract

Introduction: Osteosarcoma (OS) is a primary bone tumor that frequently metastasizes to the lung. Growing evidence suggests that primary tumors evoke phenotypic changes in resident lung fibroblasts, forming a supportive pre-metastatic niche (PMN) that favors the colonization and development of lung metastasis. Herein, we evaluated the modulation of the lung microenvironment and the reciprocal effects of reactive fibroblasts over tumor cells before lung colonization.

Material and Methods: Mice lungs were harvested from untreated animals, treated with the secretome from 143B OS cells, and mice bearing a subcutaneous primary tumor. The modulation of the extracellular matrix (ECM) proteins, collagen I/III and fibronectin were evaluated by immunohistochemistry and western blot. Lung fibroblasts were then isolated from the three different conditions and assayed for the expression of activation markers (α-SMA, vimentin, and fibronectin) by immunofluorescence and western blot. The migratory capacity of lung fibroblasts was also evaluated through a scratch assay. Inflammatory cytokines expression was also evaluated by qRT-PCR in lung tissue and lung fibroblasts. Afterward, the 143B cells were then exposed to the secretome of normal (NFs), activated fibroblasts derived from mice treated with 143B cells secretome ($NAFs^{SCR}$) and from mice bearing a subcutaneous tumor ($NAFs^{SCT}$) for different time points. These tumor cells were tested for the chemosensitivity to doxorubicin using a colorimetric resazurin assay and stemness-related features by a sphere-forming assay, and pluripotency genes and Wnt target genes expression by qRT-PCR. The induction of a dormancy state was assessed through western blot. OS cells adhesion to fibronectin was analyzed in the presence and absence of a neutralizing anti-integrin β1 antibody.

Results: Lung tissue from both treated animal models displayed increased deposition of reticulin fibers (collagen I/III) and fibronectin, and lung fibroblasts expressed α-SMA, vimentin, and fibronectin, along with an increased up-regulation of inflammatory

mediators suggesting an activated state. 143B OS cells became more resistant to doxorubicin after being exposed to the $NAFs^{SCR}$ and $NAFs^{SCT}$-derived secretome and acquired stem-like cell features, namely increased expression of SOX2 and KLF4, and enhanced sphere-forming efficiency and diameter. At 24h, 143B cells entered into a dormancy-like state, as shown by a $p38^{high}/pERK^{low}$ ratio that progressively switched to a $p38^{low}/pERK^{high}$ proliferative phenotype. The $NAFs^{SCR}$ and $NAFs^{SCT}$-derived secretome also stimulated integrin-β1-mediated adhesion of 143B cells to fibronectin.

Conclusions: OS 143B cells, through the release of biomolecules, induce alterations in the lung parenchyma and promote the activation of fibroblasts, which have reciprocal effects on tumor cells, favoring their ability to survive chemotherapy, exploit the dormancy state before engaging in a proliferative state and enhance their adhesion properties. These findings provide evidence of mutual interaction between fibroblasts and tumor cells before the onset of lung colonization. Furthermore, some of these fibroblast-mediated mechanisms provide potential targets to prevent lung metastasis formation.

Keywords: Osteosarcoma, lung metastasis, pre-metastatic niche, fibroblasts, secretome.

List of acronyms

ABC transporters	ATP-biding cassette transporters
ALDH	Aldehyde dehydrogenase
ALP	Alkaline phosphatase
APC	Adenomatous polyposis coli gene product
ATCC	American Type Culture Collection
AXIN2	Axis inhibition protein 2
BCA	bicinchoninic acid
bFGF	human basic fibroblast growth factor
BSA	Bovine Serum Albumin
CAFs	Cancer-associated fibroblasts
cDNA	Complementary DNA
CK1	Casein kinase 1
CKAP	Cytoskeleton-associated protein
CM	Conditioned medium
CRD1	Cysteine-rich domain 1
CRD2	Cysteine-rich domain 2
CSCs	Cancer stem-like cells
DKK-1	Dickkopf-1
DMEM	Dulbecco´s Modified Eagle Medium
DNA	Deoxyribonucleic acid
DOX	Doxorubicin
DTT	Dithiothreitol
Dvl	Cytoplasmic disheveled
ECM	Extracellular matrix
EGF	Human epidermal growth factor
EMEM	Eagle's minimum essential medium

EMT	Epithelial-mesenchymal transition
ERK	Extracellular signal-regulated kinase
EVs	Extracellular vesicles
FAK	Fibronectin focal adhesion kinase
FAP	Fibroblast activation protein
FBS	heat-inactivated fetal bovine serum
FSP-1	Fibroblast specific protein
GAPDH	Glyceraldehyde 3-phosphate dehydrogenase
GSK3β	Glycogen synthase kinase 3β
HBSS	Hanks' Balanced Salt Solution
HPRT-1	Hypoxanthine Phosphoribosyltransferase 1
IL-1β	Interleukin-1β
IL-6	Interleukin-6
IL-8	Interleukin-8
ITGs	Integrins
KLF4	Kruppel like factor 4
LDH	Lactate dehydrogenase
LEF	Lymphoid enhancer-binding factor
lncRNAs	Long non-coding RNAs
LOX	Lysyl oxidase
LRP5/6	Low-density lipoprotein receptor-related protein 5 and 6
MAFs	Metastasis-associated fibroblasts
miRNAs	MicroRNA
MMPs	Matrix metalloproteinases
MRI	Magnetic resonance imaging
mRNAs	Messenger RNAs
MSCs	Mesenchymal stem cells
NAFs	Normal-activated fibroblasts
$NAFs^{SCR}$	Normal-activated fibroblasts derived from mice treated with the secretome of 143B cells

$NAFs^{SCT}$	Normal-activated fibroblasts derived from mice bearing a primary subcutaneous tumor
NANOG	Nanog homeobox
NFs	Normal fibroblasts
NF-κB	Nuclear factor kappa light chain enhancer of activated B cells
OCT4	Octamer-biding transcription factor 4
OS	Osteosarcoma
PDGF	Platelet-derived growth factor
PDGFRs	Platelet-derived growth factor receptors
PET/CT	Positron emission tomography
PI3K	Phosphoinositide 3-kinase
PMN	Pre-metastatic niche
qRT-PCR	Real-Time Quantitative Reverse Transcription PCR
RIPA	Radio Immuno Precipitation Assay buffer
RNA	Ribonucleic acid
SDS	Sodium dodecyl sulfate
SDS-PAGE	Sodium Dodecyl Sulphate Polyacrylamide Gel Electrophoresis
SOX2	SRY-related HMG-box-2
Src-kinases	Non-receptor tyrosine kinase
TCF	T-cell transcription factor
TGF-β	Transforming growth factor β
TGF-βRI	Transforming growth factor β type I receptor
TGF-βRII	Transforming growth factor β type II receptor
TLR	Toll-like receptors
TME	Tumor microenvironment
TNF-α	Tumor necrosis factor α
uPAR	Urokinase-type plasminogen activator receptor
VEGF	Vascular endothelial growth factor

YWHAZ	Tyrosine 3-Monooxygenase/Tryptophan 5-Monooxygenase Activation Protein Zeta
α-SMA	α-smooth muscle actin
β-Trcp	Beta-transducin repeats-containing proteins

List of figures

List of tables

Index

1. Introduction

1.1 Osteosarcoma

Osteosarcoma (OS) is a malignant bone tumor derived from primitive bone-forming mesenchymal tissue[1], and it accounts for 20% of all cases of primary malignant bone tumors in the world[2]**.** While categorized as a rare tumor, most patients diagnosed with OS are children and adolescents in their early adulthood, which underscores the potential for life-changing consequences in this vulnerable population[3]**.** Specifically, OS has a bimodal age distribution, with the first peak at 15–19 years of age (8 cases/million/year) and the second at 75–79 years (6 cases/million/year)[4]**.** Males are slightly more affected than females in all age groups[5]. This particular incidence in young ages is due to intense linear bone growth. OS frequently localizes on long bones, especially in areas with the most rapid growth, such as arms and legs, knees, and shoulders, and particularly the distal femur, proximal tibia, and proximal humerus[5,6]**.** Inherited cancer predispositions syndromes, disruptions in several signaling pathways, and the appearance of genetic syndromes are more prone to developing OS. Li-Fraumeni (autosomal dominant mutation in the TP53 gene), hereditary retinoblastoma (RB gene), Werner, or Bloom syndromes are examples of these syndromes[7]**.** Nevertheless, OS development appears as a sporadic event in most cases (95%). Overall, poorly defined oncogenic events associated with high cellular heterogeneity of tumor cells make the new molecular therapies development extremely difficult[8]. Elderly individuals have a higher incidence of OS related to Paget disease or consequence of treatment for different cancer with a history of radiation exposure[9].

The hallmark symptoms of OS include local pain, limited joint movement, and swelling of the affected area. These symptoms can appear at any stage of the disease. The diagnosis of OS is based on a set of clinical evaluations and radiological examination[4,10]. Although the low specificity and sensitivity, alkaline phosphatase

(ALP) and lactate dehydrogenase (LDH) are the most common serum markers used for diagnosing OS[11]. In terms of imaging, MRI and PET/CT are the most advanced techniques for an OS diagnosis[12].

Histopathologically, OS is defined as a malignant mesenchymal tumor in which the tumor cells produce osteoid and bone matrix. There are several different histologic subtypes of osteosarcoma, including conventional, telangiectatic, small cell, high-grade surface, secondary, low-grade central, and periosteal and parosteal[13], but the most frequent high-grade type of this tumor is conventional OS, which represents 75% of all cases. The conventional high-grade OS can be classified by its predominant matrix as osteoblastic, chondroblastic, or fibroblastic, comprising no clear differences in clinical outcome[5,14,15].

Clinically, OS can be divided into two stages: localized and metastatic. The localized disease affects only the bone and the tissues next to the bone in which it developed[16]. Further, it can be subdivided into resectable and non-resectable, depending on the success rate of surgical removal of the tumor. The metastatic stage of OS is characterized by the spread of tumoral cells to secondary organ sites, being extremely difficult to treat with conventional chemotherapy, commonly used for the last decades[17].

When OS is diagnosed, about 15-20% of patients already have macroscopic evidence of metastases[14]. The most common site for OS metastasis is in the lungs[18], representing 85-90% of all OS metastatic disease. Sometimes it could appear in the bone (8-10%) and more rarely in the lymph nodes[19]. The remaining 80-90% of patients can be assumed to have micrometastases that are still subclinical or undetectable using current diagnostic methods[20].

OS treatment requires a multidisciplinary approach constituted by neoadjuvant chemotherapy, surgical resection, and subsequent post-operative or adjuvant chemotherapy. This chemotherapeutic approach has improved the overall survival in OS patients with nonmetastatic disease at the initial diagnosis by 70%[21]. However, this did not improve the outcome for patients harboring metastases at diagnosis or those with relapsed disease[22]. Although the 5-year survival rate in patients with localized OS reaches 70–75%, patients with metastatic disease or relapsed osteosarcoma have

remained virtually unchanged over the past 30 years, with an overall 5-year survival rate of about 20% (Figure 1.1)[23].

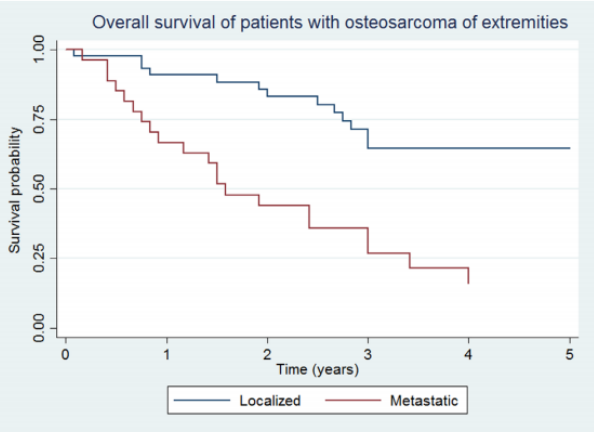

Figure 1.1 – Overall survival of patients with localized and metastatic osteosarcoma. Adapted from [23].

The current conventional treatment includes the use of three main cytotoxic agents: cisplatin, doxorubicin, methotrexate, designed as the MAP treatment[24]. Multiple efforts to improve therapeutic efficacy, including several cooperative international clinical trials, have not identified more effective or less toxic regimens, despite efforts to intensify treatment and modulate immune responses[25].

In recent years, immunotherapy has shown to be effective for treating several cancers, and its use is continually increasing. Immunotherapy is also expected to be used for OS treatment. Although several improvements, single-agent immunotherapy in clinical trials still have poor outcomes, mainly because of the immune-suppressive tumor microenvironment[2,24]. DNA and RNA analysis has also gained the researcher's attention, specifically on the somatic copy-number alteration present in the OS genome[26], but still with no significant clinical results. With these unchanging numbers in the improvement of patient survival for the last three decades, it is urgent to create new treatment strategies to improve OS patients' outcomes and survival rates and unveiling new therapeutic targets for patients with metastatic disease.

1.2 Pre-metastatic niche and metastasis formation

Metastasis is the process in which cancer cells spread from the primary site to distant organs and remain the major cause of cancer-related deaths, despite therapeutic advances in recent years[27]. The tumor cell dissemination to distant organs is a complex multistep process[28], where is created a permissive and supportive microenvironment designed as a pre-metastatic niche (PMN). The PMN is formed by the primary tumor cells to allow its efficient survival and colonization of the hostile microenvironment[29]. The original concept of the PMN appears with the hypothesis of 'seed and soil' by Stephen Paget in 1889[30], which considers that metastasis is dependent on the interactions between "seeds" (or the cancer cells) and the "soil" (or the host microenvironment). This was the first time that the requirement for a supportive microenvironment, or "fertile soil" in metastatic outgrowth, was recognized[31].

Cancers with a propensity to metastasize do not invade passively in all organs, which indicates that only a limited number of distant secondary sites provide a suitable stromal environment for their colonization[28]. This conclusion was also made by Isaiah Fidler in 1976, which demonstrated that successful metastatic colonization could occur only at certain organ sites[32]. Additional fundamental discoveries revealed that tumors induce the formation of microenvironments in distant organs that are conducive to the survival and outgrowth of disseminated tumor cells before the initiation of the metastasis. The PMN formation is regulated by several secreted bioactive factors, including growth factors and inflammatory cytokines, chemokines, and extracellular vesicles, such as exosomes, released by the primary tumor[33]. These tumor-derived secreted factors induce changes in distant pre-metastatic sites that lead to increased vascular permeability, remodeling in the extracellular matrix (ECM), reprogramming resident stromal cells, such as fibroblasts, and recruitment immune cells (macrophages and neutrophils). These tumor-driven alterations play a crucial role in architecting a permissive environment that supports the survival and outgrowth of disseminated cancer cells leading to metastatic colonization[29].

1.2.1 Metastatic process

Cancer accounts for approximately 10 million deaths per year[34]. Metastasis is the primary cause of morbidity and mortality, comprising 90% of cancer-associated mortality rates[35]. Unfortunately, it remains poorly understood due to its complexity.

Metastasis is a complex multistep process and becomes clear that the success of the metastatic formation is not exclusively dependent on the cancer cells' properties and characteristics but also on the interplay of the metastatic microenvironment and disseminated cancer cells. This complex process involves several sequential and interrelated steps, that combined with the biochemical events, form a metastatic cascade[36]. The metastatic cascade comprises local invasion of malignant cells into surrounding tissue, intravasation, dissemination and survival in the circulation, extravasation, and colonization of the cancer cells[37].

In the first step of the metastatic cascade, tumor cells migrate away from the primary tumor and invade the surrounding tissues[38]. This stage is initiated by the activation of several signaling pathways that leads tumor cells to secrete bioactive factors, for example, angiogenic factors, growth factors, such as transforming growth factor β (TGF-β), and a variety of cytokines that will allow the degradation of the basement membrane and tissue remodeling of the stromal space, favoring cancer cell invasion[28,36]. Then, they interact with the basement membrane and endothelial cells to intravasate into the bloodstream and travel in the circulation. This process is promoted by multiple intrinsic factors comprising effects via several cell types, such as fibroblasts, neutrophils, and the macrophages biding, causing a transient permeability in the vasculature[39]. Most cancer cells die in this step as a result of hydrodynamic physical damage or leukocyte attack[28]. In this stage, cancer cells should undergo a particular type of apoptosis called anoikis[40]. Anoikis is triggered by a lack of survival signals generated from the ECM and neighboring cells. This process is crucial to prevent normal cells from surviving in circulation and growing in the wrong sites[41]. This apoptotic procedure has been described to provide a barrier to cancer metastasis and has been reported an increased resistance of OS cells to anoikis, facilitating metastasis

formation[42]. In the last years, the restoration of anoikis sensitivity has been described as an effective and crucial target to inhibit metastasis.

Although these several complications on the metastatic cascade, some circulating cancer cells can extravasate out of the bloodstream and adapt, suffering an adaptation process to the new microenvironment, to colonize and proliferate, allowing the metastatic outgrowth (Figure 1.2).

The metastatic formation is a highly inefficient process, where only 0.01% of the tumor cells pass through all these steps, arrive at the PMN, and start proliferation, followed by tumor outgrowth[43]. Even with this minimal percentage of success, 20-30% of OS patients without metastasis at diagnosis will develop pulmonary metastasis during the progression of the disease.

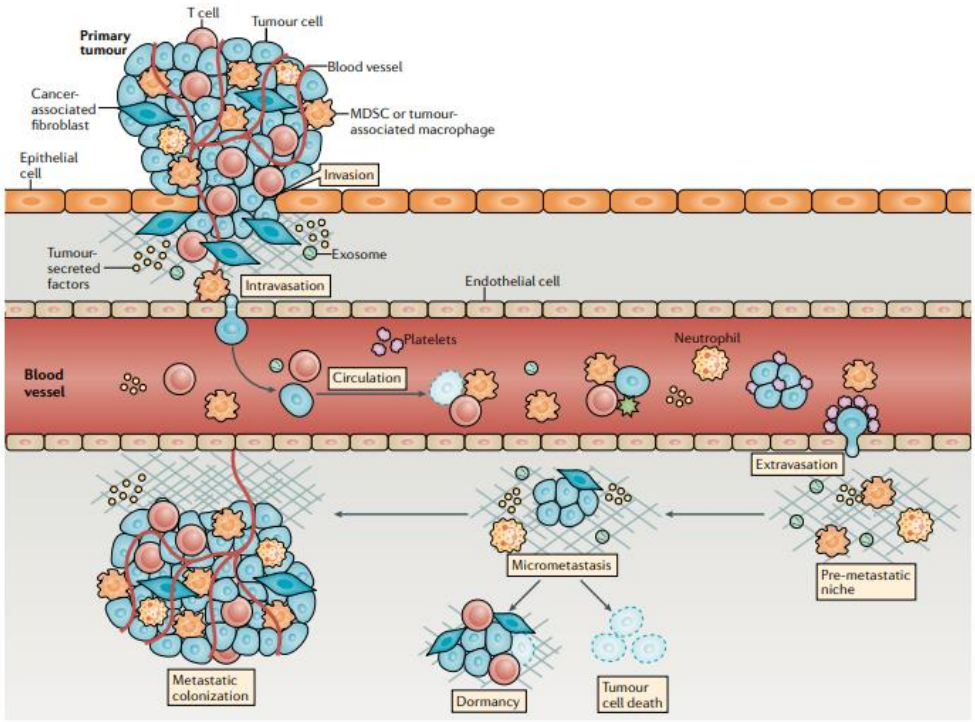

Figure 1.2 – Metastatic cascade. The metastatic formation is a complex multistep process comprising several molecular and physiological mechanisms between numerous cell types. This cascade can be divided into five main steps: 1) Invasion of cancer cells in the surrounding tissue; 2) Intravasation into the vasculature; 3) Circulation in the bloodstream; 4) Extravasation and 5) Colonization of cancer cells in the secondary tumoral site. Adapted from[28].

The deposition and further survival and proliferation is a key step of the metastatic cascade. This new microenvironment, as to have a suitable stromal environment to provide optimal conditions for colonization of the disseminated tumor cells, the PMN. As previously described, these favorable conditions are created through the primary tumor-derived secretome, which is not fully identified and characterized but, many efforts of several researchers are being made to describe this potential target in the metastatic disease[44,45].

In the further steps of metastatic formation, tumor cells should adapt to the new secondary site, promoting the development of micrometastasis. At this stage, tumor cells are constantly prone to cell death or undergoing a latent state, designed as dormancy. Tumor dormancy is defined as a prolonged latency period between the development of micrometastatic disease and the eventual formation of metastatic disease in the absence of a cell division explanation[46]. The dormant state will be elucidated further in this work.

Overall, this multi-stepping process considers the complexity of an entire event, increasing the difficulty of effective tumor therapy development[47]. Nevertheless, every single step of the metastatic cascade can be a potential target for new therapies creation. Several efforts have been made over the last years, but with no improvement of a significant outcome.

1.2.2 Organotropism

Metastatic organotropism describes the propensity for certain tumors to metastasize in specific organs under the control of a range of cellular and molecular mechanisms[48]. For example, breast cancer can metastasize to different sites, including bone, lung, liver, and brain, whereas prostate cancer preferably relapses in bone[49]. Accumulating evidence suggests that organotropism is regulated by bioactive factors released by the primary tumor that promote a suitable environment for the arrival of tumor cells at the secondary site.

The tumor intrinsic properties, as well as tissue affinities, systemic or local changes in the organ microenvironment, and interaction between tumor cells and the

tumor microenvironment (TME), have all been identified as essential factors to determine the distant organ infiltration and colonization[50]. The dynamic interactions of tumor cells with their microenvironment are crucial for cancer cell progression and metastasis. Thus, extensive cancer research has provided robust data on these interactions to understand the mechanisms underlying this cellular and molecular communication[51].

The TME is a complex environment formed by several cell types, including endothelial cells, fibroblasts, immune cells, such as macrophages and neutrophils, and non-cellular components of ECM, such as collagen, fibronectin, laminin, among others[52,53]. In this environment, tumor cells regulate the function of cellular and non-cellular components to benefit the tumor progression and metastatic spread.

Moreover, different factors are released from cancer and stromal cells, leading to alterations in distant sites and resulting in a favorable scenario for the formation of a PMN[54]. This complex network includes growth factors, such as TGF-β and vascular endothelial growth factor (VEGF), and inflammatory cytokines, like tumor necrosis factor α (TNF-α)[55]. Several other chemokines are also released, as well as extracellular vesicles (EVs), namely exosomes[56].

Exosomes are a subset of extracellular vesicles with a size range of 30–150 nm, commonly found in blood, urine, saliva, and other bodily fluids and secreted by most eukaryotic cells[57]. They are essential mediators of intercellular communication since they transmit information to target cells through their cargo levels, including proteins, lipids, DNA, messenger RNA, and microRNAs[58]. Different research groups have evaluated exosomes' influence in the modulation of the PMN and their ability to induce specific organ-directed metastasis[51]. Hoshino et al. reported that small EV-derived integrins (ITGs) dictate organ-specific targeting, thus determining organotropism to specific organs, particularly the lung, liver, and brain[33]. Small EV-derived ITGα6β4 and ITGα6β1 specify primary lung metastasis, while ITGαvβ5 directs metastasis to the liver and ITGβ3 to the brain[33,50]. The uptake of these EVs with the expression of these specific integrins induced the upregulation of genes associated with migration and inflammation.

As previously reported in the osteosarcoma case, approximately 90% of metastasis is localized in the lung[18,59,60].

The lung is a permissive organ to the metastatic development originated by several cancer types, for example, sarcomas, breast, colorectal cancer, and melanoma (Figure 1.3). Its physiology makes it ideal for colonization and metastasis, specifically the broad surface area, numerous capillaries, and high oxygenation provide good opportunities for cancer cells to adhere, extravasate, and colonize the secondary site[61]. Additionally, exosomes proteomics revealed distinct integrin expression patterns in which integrins α6β4 and α6β1 are favorably taken up by lung fibroblasts and epithelial cells, promoting the increased expression of inflammatory genes and lung metastatic development[33,62]. Furthermore, tumor-derived EVs can activate Toll-like receptors (TLR), such as TLR3, and increase cytokine secretion from epithelial cells. These cytokines arouse the recruitment of neutrophils, favoring lung metastasis[63]. Preferentially, EVs are caught by pulmonary resident fibroblasts, which acquire an activated phenotype that promote lung metastasis[62,64].

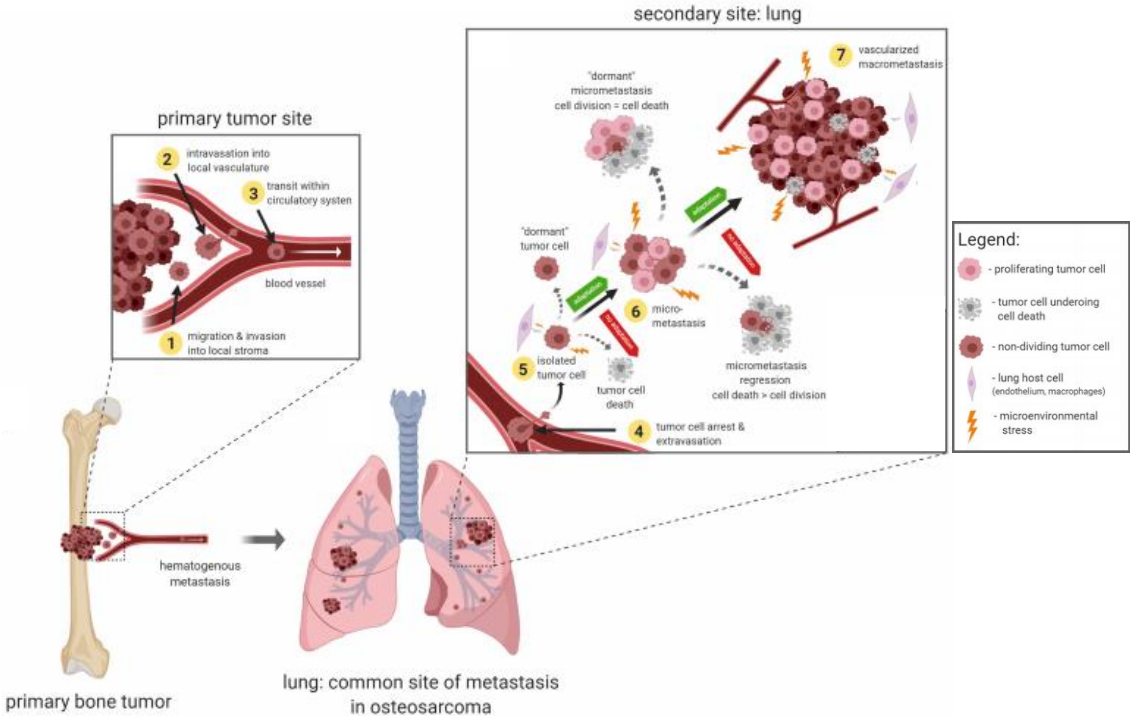

Figure 1.3 – Organotropism in osteosarcoma. Cancer cells migrate and invade the local stroma (1) and intravasate into the vasculature (2). After surviving the extreme stress in the bloodstream (3), these cells extravasate to further colonization of the lung (4). Upon the arrival to the lung (the primary site for

osteosarcoma metastasis), cancer cells interact with the organ microenvironment and the resident stromal cells (5). Cancer cells are constantly subjected to microenvironmental stress, risking cancer cell death or entry into a dormant state. They must be able to adapt and survive. In the successful management of this process, cancer cells can proliferate into multi-cellular micrometastases (6). Finally, these micrometastases recruit local blood vessels and form a vascularized secondary tumor (7). Adapted from [3].

In sum, tumor-derived exosomes are fundamental for the communication between the primary tumor and the host microenvironment, being responsible for several phenotype alterations on the secondary site. The integrins present in its membrane are essential for their recognition and internalization by the stromal cells present in the host microenvironment. After their uptake by the recipient cells, exosomes can modulate the pre-metastatic niche through many pathways including promotion of pro-inflammatory genes expression and cytokines secretion, the direction of phenotype-specific induction or differentiation, and recruitment of specific cell types.

Unraveling the importance of exosomes in the metastatic formation and organotropism, as well as the mechanisms involved, has turned into a massive study area. The translation of this knowledge can be highly beneficial to cancer management in the clinic.

1.2.3 Fibroblast's activation in the PMN formation

The interplay between cancer cells and the host environment is a crucial aspect of the formation of the PMN. Nowadays, fibroblasts are recognized as an essential cell type involved in this intercommunication, being the most abundant cells in the stroma. As a response to a stimulus provided by the cancer cells, fibroblasts become activated, exhibiting myofibroblasts characteristics that favor invasive growth and metastasis[65]. However, this cellular activation mechanism of healthy fibroblasts is not fully understood.

Fibroblasts represent a heterogeneous population of mesenchymal cells characterized by extraordinary phenotypic plasticity, the ability of secretion of various soluble factors, and regulation of inflammation[66]. These cells, under physiological conditions, can regulate the turnover of the ECM, altering the expression of many ECM constituents such as type I, III, and V collagen, laminin, elastin, and fibronectin, and control tissue homeostasis[67]. Fibroblasts are also an important source of ECM-degrading proteases such as matrix metalloproteinases (MMPs) and participate in wound healing and senescence[66,68]. In the TME, normal fibroblasts (NFs) differentiate to cancer-associated fibroblasts (CAFs) through an activation process. This activation is a consequence of the coevolution of the disorder and alterations in the biochemical and physical structure in the TME promoted by the cancer cells[69].

CAFs can be derived from bone marrow-derived progenitor cells but are mainly derived from NFs in the surrounding tissue[70]. These fibroblasts are responsible for remodeling the ECM during tumor progression and metastasis[71], where they actively participate in proteolysis, crosslinking, facilitating malignant cell migration and invasion. Furthermore, CAFs also interact with other cells in the TME through direct cell-to-cell contact and paracrine signaling[72,73]. Several intracellular signaling pathways, including the activation of TGF-β[65], PDGF, and PI3K, are reported to regulate the activity of CAFs by reprogramming the NF-κB, ERK, AKT signaling pathways[70,74]. For the fibroblasts' active phenotype characterization is commonly used some molecular markers, such as the α-smooth muscle actin (α-SMA), fibroblast activation protein (FAP), podoplanin, vimentin, fibroblast specific protein (FSP-1), and platelet-derived growth factor receptors (PDGFRs)[75]. Another crucial process for CAFs differentiation is metabolic reprogramming, which is linked to several processes, including cancer-cell induced oxidative stress, which modifies mitochondrial function, resulting in higher glucose uptake and reactive oxygen species, culminating in CAFs differentiation[66,73] .

As previously referred, CAFs are highly associated with cancer, being a dominant component of the tumor stroma. However, stromal fibroblasts at metastatic sites can be designed as metastasis-associated fibroblasts (MAFs)[76]. MAFs and CAFs share multiple functions in primary tumors, however despite this similarity, their effects on

tumor progression are not equivalent, which might be related by the different environments in which they developed[76,77].

MAFs have an increased ability to enhance the proliferation and migration level of tumor cells, induce angiogenesis, and suppress immune cells[76]. Although the effects of CAFs in primary tumors have been widely investigated, the influence of MAFs in metastatic tumors and their microenvironment have yet to be fully understood.

MAFs are highly present in the lung PMN and possibly originate from resident fibroblasts, bone marrow-derived MSCs, or CAFs from primary tumors[78]**.** Primary lung fibroblasts and established lung fibroblast cell lines can be activated in response to certain stimuli, such as EVs derived from tumor cells or from CAFs in primary tumors[79]. The incubation with the conditioned medium from tumor cells can induce the differentiation of MSCs into fibroblasts, and *in vivo* studies revealed that this transition occurs within the metastatic microenvironment[80]. In addition, stromal cells, such as fibroblasts, endothelial, or tumor-infiltrated myeloid cells, derived from primary tumors may also be part of MAFs at metastatic sites[78].

EVs, and especially exosomes, are another crucial source of activating factors of MAFs[81]. The ability of cancer-derived exosomes to promote an active phenotype in fibroblasts has been linked to several types of molecular cargo, including miRNAs, proteins, and to a lesser extent, messenger RNAs (mRNAs) and long non-coding RNAs (lncRNAs)[73,82]. This specific cargo can also influence a pro-angiogenic or pro-inflammatory phenotype in the activated fibroblasts, the induction of therapy resistance, and pre-metastatic niche formation[83].

MAFs are abundant in metastatic sites and are an important part of the PMN. MAFs can create a tumor-friendly microenvironment through the upregulation of the expression of fibronectin to promote the adhesion of cancer cells[77,84]. They can also enhance the malignant characteristics of metastatic tumor cells as well as regulate angiogenesis and immune cell migration. The appearance of an inflammatory phenotype, specifically associated with the activation of IL-6, IL-8, and IL-1β, is associated with substantial expansion of MAFs during the growth of macrometastasis[85]. This characteristic is due to an impressive increase in fibroblast proliferation. Additionally, MAFs can also induce ECM remodeling of the metastatic

site by increasing the levels of fibronectin, lysyl oxidase (LOX), and matrix metalloproteinases such as MMP9[76]. These fibroblasts can also affect the metastatic tumor cells and induce their malignant phenotypes through the maintenance of cancer stem cells (CSCs)[86], and activation of signaling pathways such as the Wnt pathway [87].

Although the numerous similarities between CAFs and MAFs, they represent a heterogeneous group of mesenchymal cells[88]. Therefore, the enlarged fibroblast population in lung metastases may include several subtypes of fibroblasts with diverse origins and functions[77], suggesting that tumors may harbor several different fibroblast subtypes in differential activation states. Thus, the role of distinct fibroblast subgroups in the metastatic progression is not fully understood, comprising the need for new studies in this area.

The fibroblasts activation is a multi-stepping process that involves several cellular, biochemical, and molecular programs[89] (Figure 1.4). The activation of NFs into MAFs can have an intermedium state, where fibroblasts present some activated features but are not *true* MAFs. These fibroblasts, designed as normal-activated fibroblasts (NAFs), display some features of MAFs, namely the expression of α-SMA and vimentin, among others activation markers, and become stellate in shape[90]. They have enhanced ECM production, suffer cytoskeletal rearrangements, and gain contractile properties. The acquired synthetic functions are associated with secretory and migratory functions that amplify their activation, recruitment, and proliferation[85]. The reversibility of such activation may be mediated by reprogramming or apoptosis of the wound healing-associated activated fibroblasts when the repair process is complete[90]. Contrary to NAFs, MAFs are associated with constant stimuli, such as the development of cancer lesions. These fibroblasts have improved ECM remodeling ability, leading to a robust autocrine activation and modulation of the immune system-related signaling pathways[91].

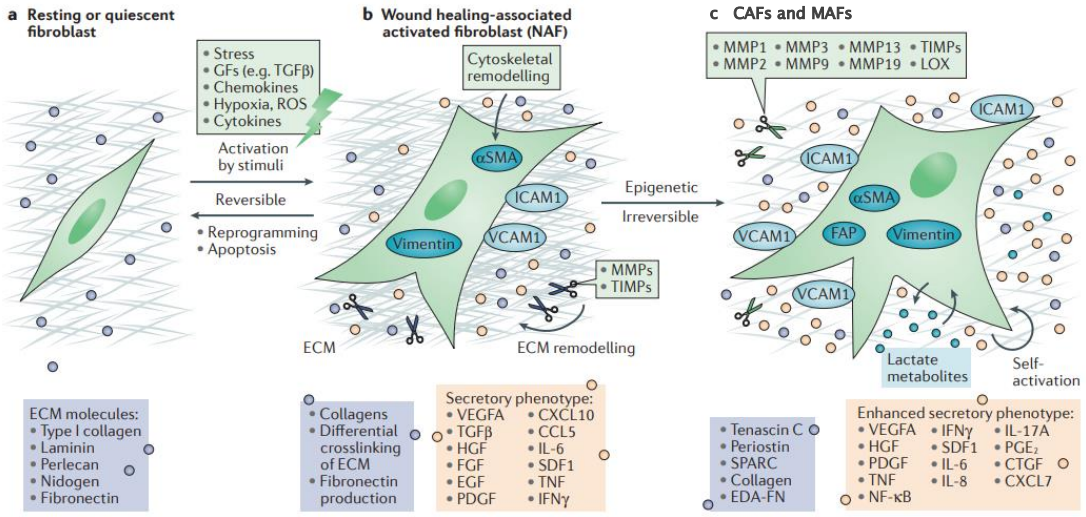

Figure 1.4 – Activation of fibroblasts. Representation of a multistep process that complies the activation of resting or quiescent fibroblasts (a) into a wound healing-associated activated fibroblast, also designed as normal-activated (NAFs) (b). The NFs activation can be stimulated by the primary tumor-derived secretome, which includes chemokines, cytokines, and several growth factors, such as TGFβ. The NAFs phenotype is reversible through cellular reprogramming mechanisms and apoptosis. Another feature of this state is the ECM remodeling, characterized by the production of collagen and fibronectin with differential crosstalk. The expression of the activation markers α-SMA and vimentin is also increased at this stage. The activation process can reach an irreversible phase promoted by epigenetic factors associated with cancer or metastatic lesions (c). CAFs and MAFs present an enhanced secretory phenotype and the ability of self-activation. Metabolic reprogramming is essential at this stage, considered a crucial factor to CAFs and MAFs differentiation. Image adapted from [89].

1.3 Cancer cell stemness, therapeutic resistance and metastasis

Growing evidence confirmed the presence of tumor cells with stem-like properties in many cancer types including osteosarcoma. These cells, as will be described in the following sections, are considered the driving force behind therapy resistance, cancer recurrence and metastasis.

1.3.1 Cancer stem-like cells (CSCs)

CSCs define a small and unique subset of cells with self-renewal ability and the capacity to generate the different cell types that constitute the whole tumor[92]. This definition has been based on their differentiation ability to form a diversified heterogeneous population and their capability to control homeostasis by modulating self-differentiation and proliferation according to environmental stimuli and genetic obstacles[93]. These cells are also referred to as tumor-initiating cells and present a therapeutic target that deceives conventional treatments to the tumor bulk[94].

Evidence exists that OS patients may develop distant metastases years after the conclusion of their first treatment, potentially highlighting the tumorigenic characteristics of CSCs, although this currently remains speculative[86,95].

Several methods have been developed to identify, isolate, or enrich subpopulations with stem cell properties within the tumors[96]. Frequently, to evaluate the cancer cell resistance properties, side population analysis (dye exclusion assay) and aldehyde dehydrogenase (ALDH) activity are assessed to enrich CSCs with these characteristics[95]. In OS, an increased rate of side population cells was shown in human primary samples, showing an upregulation on ATP-biding cassette (ABC) transporters, Oct4, and Nanog gene expression[97]. The activity of certain ABC transporters mediates drug efflux, preventing the intracellular accumulation of chemotherapeutic agents at toxic levels[98]. On the other hand, the activity of the drug-detoxifying enzyme ALDH is also a frequently used approach to evaluate CSCs chemoresistance phenotype[99]. Cancer cells with higher ALDH expression were also detected in human osteosarcoma samples, and increased ALDH activity was further correlated to metastatic potential[100,101].

In addition, Martins-Neves *et al.* described a detailed study using a sphere-forming assay as the principal CSC selection method to evaluate the presence of CSCs in OS[98]. Another study revealed that heterogeneous CSC sub-populations may exist side by side in the same cancer cell line and that different initial CSC enrichment methods allow the evaluation of the heterogeneity present within the OS CSC populations[102].

Moreover, CSCs are commonly isolated by sorting cells according to the expression of specific surface markers associated with stemness. However, a consensus is far from being achieved with several groups identifying unrelated biomarkers, which warrant a broader validation. The lack of specific OS markers can be explained by the difficulties in identifying a consistent and representative phenotype for OS[103,104]. The use of functional methodologies is still principally used, compared to molecular markers that may not be specific on their own. The expression pluripotency-related transcription factors are still the most reliable markers for CSCs identification (Figure 1.5). According to Martins-Neves *et al.*, SOX2 and KLF4, two self-renewal pluripotency transcription factors, were overexpressed in different OS cell lines[102].

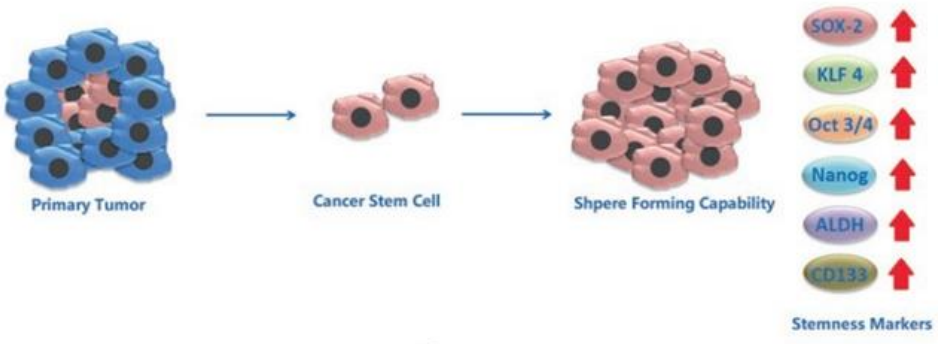

Figure 1.5 – The primary tumor contains a unique subset of cancer cells with a stem-like phenotype. CSCs can self-renew, have the capability to form spheres, and express pluripotency transcription factors such as SOX-2, KLF4, Oct 3/4, Nanog and other specific markers such as ALDH and CD133. Adapted from[105].

Several signaling pathways mediate the acquisition and maintenance of a stem-like phenotype in tumor cells.

Some studies revealed that TGF-β1 signaling combined with a hypoxic environment dramatically induced self-renewal in non-stem OS cells. This cytokine also increased the OS CSCS metastatic potential, chemoresistance, tumorigenicity, and neovasculogenesis[106]. TGF-β1 treatment also influences the expression of SOX2 immature or undifferentiated cells and increases the Nanog and Oct4 expression[94,107].

Stem cell-associated signaling pathways, such as Notch, Hedgehog, and Wnt, have also been implicated in therapy resistance and correlated with an increase in the

number of CSCs during and after treatments[108]. These signaling pathways are involved in the self-renewal and maintenance of an undifferentiated state of stem cells[109]. Any dysregulation in these pathways can result in the cells' acquisition of a stem-like phenotype [110,111]. Wnt pathway activation in CSCs has been extensively explored in a wide variety of cancers[112]. Specifically, in OS, some studies revealed that the Wnt signaling pathway is active, contributing to the emergence and maintenance of the stem-like phenotype[113]. This pathway will be further detailed explained.

In sum, CSCs have a critical role in metastasis and are considered to be the ones to have epithelial-mesenchymal plasticity[114]. There is no doubt that the microenvironment at the primary and secondary tumor sites plays a decisive role in whether cancer cells acquire an invasive phenotype and invade the tumor stroma and establish themselves in a distant host environment[115]. Different approaches to combat metastasis targeting CSCs have been proposed and tested. These methods include modulation of the microenvironment, differentiation therapy, immunotherapy, and cancer stem cell-specific signaling pathways inhibition.

1.3.2 Wnt/β-catenin signaling pathway

The Wnt signaling pathway is described to play a pro-oncogenic role by stimulating cell proliferation and motility[116]. Additionally, this pathway has a crucial role in regulating CSC function[117,118]. In osteosarcoma, stem cells have activated Wnt/β-catenin signaling, and Wnt inhibition can consequently reduce drug resistance[119].

This signaling pathway can be activated through a canonical or noncanonical pathways with different signaling cascades[120]. In contrast to the noncanonical pathways, which are independent of β-catenin, the canonical pathway regulates the transcriptional coactivator β-catenin function. Also, the canonical Wnt/β-catenin pathway is required for osteoblast differentiation, enhanced ossification, and suppression of chondrocyte formation during bone development[105]. Moreover, the abnormal activity of this pathway in OS cells plays an essential role in tumorigenesis and metastasis[121].

The Canonical Wnt Pathway

In the absence or inhibition of Wnt ligands, the cytoplasmic β-catenin forms a complex with multiple proteins. This complex includes Axin, adenomatous polyposis coli gene product (APC), casein kinase 1 (CK1), and glycogen synthase kinase 3β (GSK3β)[116]. Once this complex is formed, CK1 and GSK3β phosphorylate β-catenin, which is targeted and recognized by β-Trcp, the E3 ubiquitin ligase subunit for proteasomal degradation. When Wnt ligands bind to their target membrane receptors, frizzled and low-density lipoprotein receptor-related protein 5 and 6 (LRP5/6), cytoplasmic disheveled (Dvl) causes phosphorylation of the complex, leading to an inhibition of GSK3β. This complex formation results in the cytoplasmic accumulation of non-phosphorylated β-catenin, promoting its translocation into the nucleus. Within the nucleus, β-catenin binds with the T-cell transcription factor (TCF) and the lymphoid enhancer-binding factor (LEF), forming a complex that induces the transcription of multiple downstream target genes (e.g., c-Myc, cyclin D1) that enhances cellular proliferation[105,116,122] (Figure 1.6).

Over the years, the Wnt signaling pathway has been extensively studied, resulting in the identification of several Wnt antagonists' families. Some antagonists bind directly to the Wnt ligands, but others compete for the Wnt receptors. The dickkopf (DKK) family competes with the Wnt ligand for the receptor LRP5/6[105,123]. Human DKK-1 inhibits the canonical Wnt signaling pathway by binding to the transmembrane receptor LRP5/6, preventing interaction with Wnt ligands[124]. DKK proteins have two cysteine-rich domains, cysteine-rich domain 1 (CRD1) and CRD2. More recently, it has been recognized that DKK-1 binds to LRP5/6 through the CRD1 domain and to a cytoskeleton-associated protein (CKAP) 4 through CRD2 to induce proliferation in normal and tumor cells in a β-catenin-independent manner via the PI3K/AKT pathway activation[125]. Additionally, DKK-1 has an immunomodulatory role by attenuating the canonical Wnt signaling pathway, facilitating cell-mediated immune evasion by natural killer cells[126].

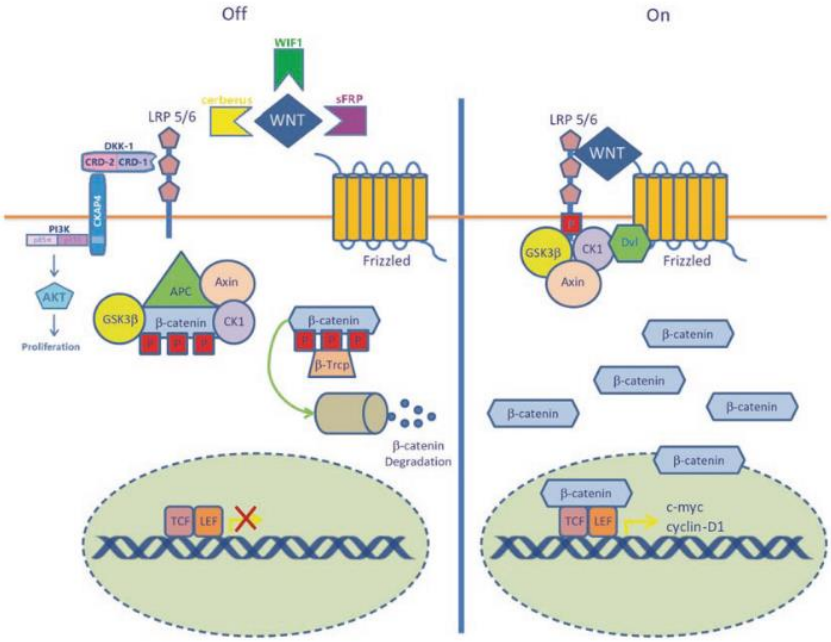

Figure 1.6 - Overview of the canonical Wnt signaling pathway. Adapated from[105].

1.3.3 Cell resistance

Cancer cells resistance has been traditionally believed to appear as a result of preexisting gene mutations. However, recent evidence points toward more dynamic and complex models occurring during tumor progression, including inactivation of drugs, improved DNA repair, modulation of signaling pathways, disruption in gene expression linked to the cell cycle, or even implication of the micro-environment and decrease in intracellular accumulation of the drugs[127].

Additionally, the mechanisms of the acquisition of a resistance phenotype are highly variable depending on the cancer type. The development of chemoresistance in malignant tumors limits the effectiveness of cytotoxic drugs, and this is particularly true in OS, which is characterized by the frequent refractoriness to chemotherapy[128]. Recent studies revealed that the expression of stemness markers related to a stem-like phenotype is crucial for tumor maintenance, being also mediators of resistance[102]. This evidence is remarkably relevant since CSCs are described as drivers of metastasis, and

metastatic tumors are associated with a more invasive and aggressive cancer phenotype[129].

Due to CSCs' increasing relevance in therapy resistance, these cells have gained intense attention recently, revealing them to be a potential target for cancer therapy. It has been described that CSCs are more resistant to radiotherapy and conventional chemotherapy when compared to the bulk cancer cells. This phenotype is a driving force behind cancer cell colonization at distant sites of metastasis despite the application of adjuvant chemotherapy[130]. CSCs are highly dynamic, heterogeneous, and easily adaptive to the surrounding environment[131,132]. They have efficient DNA repairing systems with DNA checkpoint kinases and sustained stemness features, all of which are accountable for their therapy resistance.

Additionally, CSCs have an effective drug-efflux system, with increased expression of ABC transporters, such as P-glycoprotein[133]. The epithelial-mesenchymal transition (EMT) is also a factor massively described in CSCs, considering crucial for tumor progression and resistance to therapy. The activation of the Wnt/β-catenin, Hedgehog, Notch, and PI3K/Akt/mTOR signaling are associated phenotypic changes and appearance of a resistant phenotype. These intrinsic mechanisms allow CSCs to survive current cancer therapies, initiating the reconstitution of the original tumor, long-term tumor recurrence, and metastasis[134].

CSC resistance is also influenced by extrinsic factors like the TME, through their interaction with the local surrounding heterocellular components that determine tumor fate[135]. Tumors have distinct genetic and epigenetic features, which are due in part to the contribution of the TME. Invasive mesenchymal type CSCs are mostly found in the regions of intense cellular density allowing the communication between CSCs and the TME cells[136]. Overall, these factors highlight the importance of the TME in the molecular and functional features of CSCs contributing to a therapy-resistant phenotype[130].

Although the intense research in the CSCs, the specific mechanism of OS stem cells drug resistance is still not fully clarified, posing hurdles for the development of specific targeted therapies. This still represents a critical challenge to obtain a durable clinical response with the prevention of tumor recurrence and metastasis.

1.4 Dormancy state

In many cancer patients, metastatic diseases occur following extended periods of disease-free survival, which remain a common cause of morbidity and mortality[27]. The appearance of tumor relapse after a prolonged time has been attributed to the ability of disseminated tumor cells to enter into a long-term dormant state[137].

Dormant cells can survive in a quiescent state and remain undetected for long periods, explaining the prolonged asymptomatic residual disease and treatment resistance. The designation of dormancy can be divided in the senescence of either multiple cells, called tumor mass dormancy, or individual cells, denominated cellular dormancy[138]. Cellular dormancy is a process where individual tumor cells enter in a temporarily quiescent state and stop dividing. Such cells are typically more resistant to conventional drugs because current treatments tend to target proliferating cells[139]. In this dormant state, cells exit the cell cycle and enter temporarily into a G0 phase[140]. Moreover, this is a reversible process and under certain microenvironmental conditions such as the presence of growth factors, cytokines, nutrients, or chemical agents, cancer cells may escape and re-enter the cell cycle to restart proliferation[137,141].

The molecular mechanisms underlying cellular dormancy and reactivation has been focus of intense investigation. The interactions between cancer cells and the surrounding components of the ECM have a central role in this process.

The activation of the extracellular signal-regulated kinase (ERK) has a prominent role in determining whether cells proliferate or enter dormancy. Cancer cells in a continuous proliferation state exhibit constitutive ERK activation, which allows G0-G1-S phase transition and cell division[142]. In this proliferation state, a high level of p38 activity functions as an inhibitory regulator of ERK and prevents cell proliferation by inducing G0-G1 arrest or triggering senescence and apoptosis. Indeed, *in vivo* studies revealed that the p38/ERK activity ratio can be an indicator of dormant cells in various cancer types, such as breast and prostate cancer, melanoma, and fibrosarcoma[143]. Cancer cells with $p38^{low}/ERK^{high}$ activity were highly proliferative *in vivo*, whereas those

with $p38^{high}/ERK^{low}$ activity were alive by unable to proliferate, suggesting their entry into a dormant state[143,144]. Apparently, any regulatory factor that change the balance of p38/ERK activity dictate whether cancer cells growth or remain dormant. The activation of these kinases was found to be driven by the interaction of urokinase-type plasminogen activator receptor (uPAR), α5β1 integrin, fibronectin focal adhesion kinase (FAK), and Src-kinases[137]. Several studies revealed that proliferating cells are characterized by high expression of uPAR that leads to activation of Src-kinase, resulting in the ERK1/2 phosphorylation[145]. Increased level of fibronectin also results in ERK1/2 phosphorylation. Conversely, p38 phosphorylation is favored when uPAR expression is lost and when fibronectin is absent[146].

The cytokine TGF-β is also a crucial factor in the induction of a dormant state in cancer cells. The production of TGF-β1/2 is increased during osteoblast differentiation, and it is described that this cytokine can induce cancer cell quiescence[147]. TGF-β receptor type III participates in the TGF-β1-induced dormancy and activates the phosphorylation of retinoblastoma through p38 MAPK activation[148]. Overall, these data show that many of these dormancy-inducing cytokines from the stroma, such as TGF-β and uPAR, can promote the $p38^{high}/ERK^{low}$ state, resulting in G0 cell cycle arrest and cancer dormancy in the absence of proliferative signaling.

As the principal producers of extracellular matrix components, lung fibroblasts play a crucial role in regulating the lung ECM. The lung fibroblast population is highly heterogeneous, and the aberrant expansion of specific fibroblast phenotypes contributes to ECM remodeling in lung tumors. Additionally, growth factors such as TGF-β and PDGF secreted by cancer cells and tumor-infiltrating immune cells recruit and activate fibroblasts to a myofibroblast-like state[148]. The activated fibroblasts have several transcriptional and signaling programs that promote proliferation, inhibit apoptosis and drive ECM remodeling leading to increased mechanical stiffness[149]. These fibroblasts also secrete large amounts of collagen I, collagen IV, fibronectin and are rich in cysteine, tenascin–C, thrombospondin-2, connective tissue growth factor, MMPs, and plasminogen activators[150–152]. All these factors contribute to the ECM's significant remodeling, altering the tumor behavior and its microenvironment. Moreover, the metabolic activity of activated fibroblasts has also been recognized as

an essential factor in ECM-dependent dormancy regulation. Their increased glycolytic and autophagic activity compared to normal lung fibroblasts promotes the survival and rapid proliferation of cancer cells[153]. Apparently, the crosstalk between lung fibroblasts and cancer cells can regulate the dormancy and outgrowth behavior of tumor cells.

Although a variety of signaling cascades are linked to the breaking of dormancy, these signaling networks eventually lead to a change in the balance between p38 and ERK activities in favor of ERK. Therefore, targeting this ratio to modulate the balance towards p38, might be a possibility to induce a permanent dormant state, preventing metastasis (Figure 1.7).

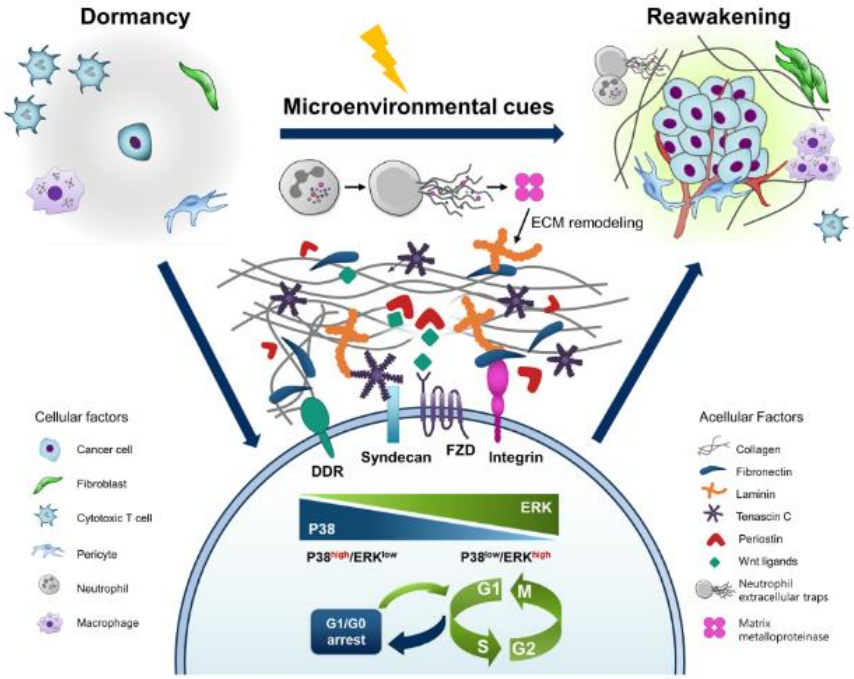

Figure 1.7 – Mechanisms of cancer cells entry and reawakening of a dormant state. Cancer cells often enter dormancy to resist and adapt to the secondary metastatic environment. Already in a new location, these dormant cancer cells receive signals from the surrounding tissue characterized by the ECM remodeling, augmenting the ability to re-enter the cell cycle, start proliferation and trigger tumor development. Adapted from[144].

In sum, the microenvironment has been increasingly recognized as a critical regulator of cancer progression, being the ECM a key component for immediate contact with the tumor cells. The ECM remodeling is a crucial factor to promote several alterations on the cancer cells phenotype, such as motility improvement,

growth, and survival, affecting tumor biology and progression[154]. Additionally, cell adhesion to the ECM triggers intracellular signaling pathways that can regulate cell cycle progression, migration, and differentiation, through integrins and other cell surface receptors[155]. Thus, integrin-mediated interactions between cancer cells and the ECM are critical modulators of the metastatic potential of cancer cells[156].

Therapeutically, targeting the crosstalk between the PMN and cancer cells is crucial for treating cancer patients and preventing metastatic spread.

1.5 Objectives

The development of metastasis initiates with a sequence of events that start earlier prior to the dissemination and local invasion of tumor cells in secondary organs, which begins with the preparation of the PMN. Knowing the molecular and cellular changes that render a distant organ hospitable for disseminating tumor cells to colonize is crucial to our understanding of the metastatic process.

The lung is the most frequent site of metastatic focus in osteosarcoma. In this work, we intend to understand how the primary tumor modulates stromal fibroblast in the lung microenvironment during the PMN formation and how the reciprocal interaction between activated fibroblasts and tumor cells might increase their metastatic behavior.

To address these questions, we propose to:

- Evaluate the effects of osteosarcoma cell-derived secretome in the activation status of lung fibroblasts during the PMN formation
- Evaluate the reciprocal effects of activated fibroblasts on osteosarcoma cells, regarding:
    - Chemoresistance phenotype
    - Acquisition of stem-like characteristics
    - Cell's ability to switch between dormancy and proliferation
    - Cell adhesion ability to ECM components.

2. Materials and Methods

2.1 Cell Culture

The human osteosarcoma cell line 143B was purchased from the American Type Culture Collection (ATCC, Rockville, MD, USA). Cells were grown in monolayer and were cultured in Eagle's minimum essential medium (EMEM; Sigma-Aldrich, MO, USA) supplemented with 10% (v/v) of heat-inactivated fetal bovine serum (FBS, Gibco, Paisley, UK), 1% (v/v) antibiotic/antimycotic solution (Sigma-Aldrich, MO, USA), 1% (v/v) sodium pyruvate (Gibco, NY, USA), 1% BrdU (v/v) (Sigma-Aldrich, MO, USA) and 2.2 g/L sodium bicarbonate (w/v) (Sigma-Aldrich, MO, USA). This cell line is stably transduced with a lentivirus encoding luciferase. Cells were maintained in a humidified atmosphere at 37°C with 5% CO_2. When cells reached an 80-90% confluence they were detached with TrypLE Express (Gibco, NY, USA), centrifuged at 1500 rpm for 5 min, and subcultivated at an appropriate ratio. All procedure involving cell manipulation was performed in sterile condition inside a laminar flow chamber.

2.2 Cell viability

Cell counting and viability were determined before each experiment through Trypan Blue exclusion method. In this method, a cell suspension is mixed with trypan blue dye and then visualized at the microscope to determine the number of viable cells. Viable cells have intact membranes that prevent cell staining, while dead cells have a blue cytoplasm.

Equal volumes of trypan blue solution (Sigma-Aldrich, MO, USA) and cell suspension were mixed (dilution 1:2) and transferred into a Neubauer chamber. Cells were observed immediately and counted using an inverted microscope.

Cell viability was calculated as the percentage of viable cells relative to the total number of cells. Only cell suspensions with viability higher than 90% were used in all the experiments.

2.3 Sphere forming assay

The isolation of stem-like cells or CSCs from the OS 143B cell line was performed using the sphere-formation assay in ultra-low attachment surfaces, as previously described[98]. In brief, 143B cells were detached with TrypLE Express (Gibco) and plated at a density of $6x10^4$ cell/well in a 6-well cell culture plate (Orange Scientific) previously coated with 0.8 mg/cm^2 poly(2-hydroxyethyl methacrylate) [poly-HEMA; Sigma-Aldrich, MO, USA] in 2 mL of N2 medium with 1% methylcellulose (Sigma-Aldrich, MO, USA).

N2 medium is composed by Dulbecco´s Modified Eagle Medium (DMEM; Sigma-Aldrich, MO, USA) supplemented with 1.2 g/L of sodium bicarbonate (Sigma-Aldrich, MO, USA), 20 nM of progesterone (Sigma-Aldrich, MO, USA), 100 µM of putrescine (Sigma-Aldrich, MO, USA), 1% (v/v) of insulin-transferrin-selenium-A supplement (Gibco, NY, USA) and 1% (v/v) antibiotic/antimycotic (Sigma-Aldrich, MO, USA). The medium was filtered and mixed with an equal volume of 2% methylcellulose previously sterilized to avoid single-cell aggregation. Human epidermal growth factor (EGF; Peprotech, CA, USA) and human basic fibroblast growth factor (bFGF; Peprotech, CA, USA) were added at 10 ng/mL every two days. Cells were kept at 37°C in a humidified atmosphere of 5% CO_2.

After 8-10 days, images of the sphere-forming colonies were taken with an inverted microscope (AE2000 Trinocular microscope, Motic) operating in bright-field mode. The diameter of the spheres was measured using the Motic Images Plus 3.0 for Windows 64-bit OS and Image J software. The sphere-forming efficiency was calculated as the number of spheres formed divided by the initial number of seeded cells and expressed as a percentage. Spheres were counted in a Neubauer chamber using the trypan blue stain (Sigma-Aldrich, MO, USA).

This assay was performed before and after preconditioning of 143B cells with the secretome of fibroblast cell populations for 48h.

2.4 Animal studies

Swiss nude mice (Swiss nu/nu mice, 8-10 weeks old) were obtained and housed under pathogen-free conditions in individually ventilated cages at the *Vivarium of the Coimbra Institute for Clinical and Biomedical Research* (iCBR, Coimbra, Portugal) of the Faculty of Medicine of the University of Coimbra. All animal experiments were approved by the Animal Welfare Committee of the Faculty of Medicine of the University of Coimbra (ID ORBEA: 11/2020) and were performed in accordance with the European Community directive guidelines for the use of animals in a laboratory (2010/63/EU) transposed to the Portuguese law in 2013 (Decreto-Lei 113/2013).

Mice were divided into three groups: I) untreated control animals; III) animals treated with the secretome of 143B cells; III) animals bearing a primary subcutaneous tumor.

The secretome preparation and protocol of administration in animals is under confidentially. The subcutaneous tumor was induced by subcutaneous injection of 143B cells ($5x10^4$/100μL PBS) into the lower flank. Tumor growth was monitored using a digital caliper twice a week until the tumor reached 1cm in diameter.

After ending the treatment with the secretome or the subcutaneous tumors reaching the 1cm diameter, the animals were euthanized by cervical dislocation, and the lungs were collected for fibroblasts isolation.

2.5 Isolation of fibroblasts and primary cultures establishment

Immediately after animals' sacrifice, the lungs were harvested and kept in a cold Hanks' Balanced Salt Solution (HBSS). The lung tissue was cut into small pieces and enzymatically digested with 5 mL of Digestion buffer (0.1% Collagenase A, 2.4U/mL Dispase, 2 mM CaCl, 10 mM HEPES, and 2.25 mL of Lysis Buffer - 150 mM NaCl, 10 mM

HEPES, 2 mM CaCl2), for 90 min at 37°C in a 5% CO_2 incubator with a gentle mix every 30 min.

The digested lung pieces were filtered through a 70 µm cell strainer (Corning Incorporated, NY, USA) and washed with PBS (w/o Ca2+) containing 0.05 mM EDTA to keep the cells separated. The cells suspension was centrifuged at 1500 rpm for 5 min, and the cells were plated into 1% gelatin pre-coated dishes and maintained in RPMI culture medium (RPMI-1640 Medium; Sigma-Aldrich, MO, USA) with 15% (v/v) FBS (Gibco, Paisley, UK) and 1% (v/v) antibiotic-antimycotic (Sigma-Aldrich, MO, USA) in a humidified atmosphere at 37°C with 5% CO_2. After 24h, cells were washed with PBS and replenished with culture medium. After reaching confluence, cells were routinely trypsinized with 0.05% trypsin/EDTA (0.1%) and maintained in RPMI medium with 15% FBS at 37°C and 5% CO_2. The primary cultures of fibroblasts established from the lungs of the three groups of animals were used until passage four.

Fibroblasts isolated from control animals were designed as normal fibroblasts (NFs). Fibroblasts isolated from animals treated with the 143B OS cells derived secretome were designed as normal activated ($NAFs^{SCR}$) and from animals bearing a subcutaneous primary tumor ($NAFs^{SCT}$).

2.6 Collection of conditioned medium from fibroblasts

Conditioned medium (CM) also known as secretome was collected from the three populations of fibroblasts as follows: cells were seeded in 10 cm dishes at a density of $5x10^5$ cell/mL and allowed to attach overnight. The next day, the culture medium was removed, and the cells were washed with PBS and incubated with exosome-free culture medium for 24h. After this period, the medium was collected and centrifuged at 1000 rpm for 5 minutes to remove cell debris and concentrated using a centrifugal filter (Amicon Ultra - 15, Merck Millipore, Co Cork, IRL). The protein content of non-concentrated and concentrated fractions was determined using the bicinchoninic acid (BCA; Sigma-Aldrich, MO, USA) method with BSA (Sigma-Aldrich, MO, USA) as a standard, and then aliquoted and stored at -80°C until use.

2.7 Histopathological analysis and immunostaining

Lung tissue was fixed in 4% paraformaldehyde and processed for paraffin embedding. Sections of 4 µm were stained with an antibody against fibronectin (ab2413; Abcam, USA). Antigen retrieval was performed by immersing slides in EDTA-Tris buffer (pH 8) for 8 min at 95 °C and then blocked with a buffered hyper protein solution for 4 min to avoid nonspecific bonds. Immunostaining was performed using a Ventana Marker Platform Bench Mark Ultra IHC/ISH with the resource of a multimeric indirect free biotin detection system - Optiview DAB IHC Detection Kit (Ventana Medical Systems, Arizona, EUA), according to the manufacturer instructions. A Gordon's and Sweet silver staining was performed for the detection of reticulin fibers which are mainly composed of type I/III collagen. Then, slides were observed under a light microscope Nikon Eclipse 50 I, and images were captured with a Nikon-Digital Sight DS-Fi1 camera.

2.8 Immunocytochemistry

Lung fibroblasts were seeded on the coverslips (12 mm; VWR, Germany) in 24-well plates, previously coated with gelatin with 0.1% of PBS, and cultured overnight. Cells were fixed in 4% paraformaldehyde for 20 min, permeabilized with 0.2% Triton X-100 (Sigma-Aldrich, MO, USA) for 10 min, and then blocked for 1 h with 3% BSA in PBS. Then cells were incubated with the following primary antibodies overnight at 4°C: Vimentin (MA5-16409) obtained from Invitrogen (1:200), α-SMA (ABT1487) from EMD Millipore (5µg/mL) and Fibronectin (ab2413) from Abcam (1:200). Finally, fibroblasts were incubated with the respective secondary antibodies: anti-rabbit (1:200) and with the nuclear marker Hoestch 33258 from Sigma-Aldrich (1:1000) for 1 h at room temperature (RT).

For immunofluorescence staining with Alexa fluor 555 Phalloidin (Abcam, 1:40), fibroblasts were fixed for 10 min with 4% paraformaldehyde containing 4% sucrose, permeabilized with 0.2% Triton X-100 (Sigma-Aldrich, MO, USA), and blocked with 1% BSA for 45 min at room temperature. The primary antibody incubation was made for

20 min at room temperature and then incubated with the nuclear marker for 5 min (Hoestch; 1:1000).

The coverslips were mounted onto microscope glass slides (Thermo scientific, USA) with a Vectashield mounting medium (Vector Laboratories, CA) and kept at 4°C until microscope view. Images were captured with a Widefield Microscope (Carl Zeiss, Göttingen, Germany) and quantified using ImageJ 1.52a (Java 1.8.0_112 [64 bit]) software (National Institutes of Health, USA).

2.9 Scratch assay

Fibroblasts were seeded at a density of $25x10^3$ cell/well in 24-well plates (Orange scientific) previously coated with 0.1% gelatin and allowed to reach a 95-100% confluence in a serum-free medium. A scratch was created in the monolayer with a pipette tip of 200 µL. The cells washed with PBS to remove cell debris and non-attached cells and were maintained in serum-free medium. Photographs were taken with an inverted microscope (AE2000 Trinocular microscope, Motic) at x4 amplification at 0, 6, and 24 hours after the scratch. Gaps area at each time-point were measured using the ImageJ software and normalized to the baseline.

2.10 Real Time-Polymerase Chain Reaction (qPCR)

RNA isolation and cDNA synthesis

Total RNA from fibroblast cell cultures and lung tissue were isolated using the TRIzol reagent.

After obtaining the cellular pellet, was added 350 µL of TRIzol (Invitrogen, UK) and incubated for 5 min with a regular vortex. After this period, 150 µL of chloroform (Merck, Germany) were added to each tube and shacked vigorously for 15 sec. The mixture was centrifuged at 13 000 rpm for 10 min at 4°C to separate the aqueous and organic phases. The aqueous transparent phase was transferred to a new RNAse-free

microcentrifuge tube and added 350 µL of 2-propanol (Merck, Germany) and gently mixed. The mixture was centrifuged again in the same conditions as previously to RNA precipitation. The supernatant was discarded, and the pellet was washed with 300 µL of 75% ethanol. The sample was centrifuged again, the supernatant removed, and the pellet left to air dry. Pellet was then dissolved in 18 µL of nuclease-free water (Nzytech, Lisboa, Portugal), and samples were quantified using nanodrop. RNA quality was evaluated based on $A_{260/280}$ and $A_{260/230}$ ratios.

For lung tissue RNA isolation, 35 to 50 mg of lung tissue was placed in a glass potter (Wheaton, USA) with 1 mL of TRIzol and homogenized in ice. All potter content was removed with a Pasteur pipette, placed in the original microcentrifuge tube, and stored overnight at 80°C. The sample was defrosted, added 200 µL of chloroform, and shacked for 15 sec. The mixture was kept on ice for 5 min and then centrifuged at 12 000 g for 15 min at 7°C. The aqueous transparent phase was carefully removed and transferred to a new RNAse-free microcentrifuge tube. After this procedure, was added 400 µL of 2-propanol and 1 µL of glycogen, and the sample stored at 20°C overnight. On the next day, the mixture was centrifuged for 12 000 g for 30 min at 4°C. The supernatant was discarded, and the pellet was washed twice with 200 µL of 75% ethanol. The sample was centrifuged again at 7500 g for 5 min at 4°C, the supernatant removed, and the pellet left to air dry. Pellet was then dissolved in 16 µL of nuclease-free water, and samples were also quantified using nanodrop, and RNA quality was also evaluated based on A260/280 and A260/230 ratios.

RNA extraction from OS 143B cells and spheres was performed using the NZY Total RNA Isolation Kit (Nzytech, Lisboa, Portugal), according to the manufacturer's instructions. RNA quality was evaluated based on $A_{260/280}$ and $A_{260/230}$ ratios. All samples were kept at -80°C until use.

cDNA synthesis was performed with 2 µg of total RNA using the NZY First-Strand cDNA synthesis kit (Nzytech, Lisboa, Portugal) according to manufacturer instructions in a C100 Thermal Cycler (BioRad, USA).

Real Time-PCR

Real Time-PCR was performed in duplicate in CFX Connect Real-time PCR detection system (Biorad, USA) using the Xpert Fast SYBR Mastermix (Grisp) in a final volume of 15 µL containing 2.5 µL of diluted cDNA. Forward and reversal primer sequences of the target and housekeeping genes used are listed in Table 2.1 and were synthetized by Eurofins Genomics. A Primer-BLAST search was performed to evaluate primer specificity and self-complementarity values of already validated and published primer sequences.

The qPCR conditions were performed as follows: initial denaturation at 95°C for 3 min, followed by 40 cycles of 30 sec denaturation at 95°C, 20 sec at 55°C for primer annealing, 20 sec at 72°C for extension cycle, followed by a final extension of 10 min at 72°C.

Transcript levels were normalized to the geometric mean of two housekeeping genes. The relative gene expression was analyzed using the $2^{-\Delta\Delta Ct}$ method and the BioRad CFX Maestro software.

The reference genes to normalize target genes in 143B, sphere-forming cells and lung tissue were the HPRT-1 and GAPDH, whereas for mice lung fibroblasts were the GAPDH and YWHAZ, ranked as stably expressed by the RefFinder algorithm (https://www.heartcure.com.au/reffinder/).

Table 2.1 - Sequences of primers used in this study.

Gene	Primer Forward (5'-3')	Primer Reverse (5'-3')	Reference
m GAPDH	GCCTTCCGTGTTCCTACC	GCCTGCTTCACCACCTTC	[157]
m HPRT-1	GTTGAAGATATAATTGACACTG	GGCATATCCAACAACAAAC	[158]
m YWHAZ	CAGCAAGCATACCAAGAAG	TCGTAATAGAACACAGAGAAGT	[159]
m TGF β	ATGGTGGACCGCAACAAC	TTGCTATATTTCTGGTAGAGTTCC	[160]
m TNFα	CAAGGGACTAGACAGGAG	TGCCTCTTCTGCCAGTTC	[161]
m IL-1β	TCTATACCTGTCCTGTGTAATG	GCTTGTGCTCTGCTTGTG	[162]
m IL-6	TTCCATCCAGTTGCCTTC	TTCTCATTTCCACGATTTCC	[161]
h GAPDH	ACAGTCAGCCGCATCTTC	GCCCAATACGACCAAATCC	[163]
h HPRT-1	TGACACTGGCAAAACAATG	GGCTTATATCCAACACTTCG	[163]
h SOX2	CATGCACCGCTACGACG	CGGACTTGACCACCGAAC	[102]
h KLF4	CCACACTTGTGATTACGCGG	TACGGTAGTGCCTGGTCAGT	[102]
h OCT4	TCTGCATCCCTTGGATGTGC	GTGTGGCCCCAAGGAATAGT	[102]
h NANOG	GATGCCTCACACGGAGACTG	GCAGAAGTGGGTTGTTTGCC	[102]
h LRP5	ACAACGGCAGGACGTGTAAG	AGCACGATGTCGGTGAAG	[119]
h LRP6	AGGGTGGAATGAATGTGCTT	TGATGGCACTCTTTTGACTGA	[119]
h AXIN2	GAATGAAGAAGAGGAGTG	AAGACATAGCCAGAACC	[119]
h DKK-1	CCTTGGATGGGTATTCCAGA	CCTGAGGCACAGTCTGATGA	[119]

2.11 Western Blot Analysis

In the lung tissue samples derived from untreated mice, treated with 143B cells-derived secretome and mice bearing a primary tumor was evaluated the expression of fibronectin an extracellular matrix protein.

The expression of fibroblast activation markers (α-SMA and Fibronectin) and the TGF-β receptor type II (TGF-βRII) was analyzed in fibroblasts collected from untreated, secretome-treated and mice carrying a subcutaneous tumor.

To evaluate the effects of the fibroblasts-derived secretome on the induction of stemness features and 143B cells entry in a dormant state, these cells were incubated with NFs, $NAFs^{SCR}$ and $NAFs^{SCT}$-derived secretome and evaluated the expression of β-catenin, pERK, p-p38 and integrin β1 expression levels.

Preparation of cellular extracts

Total cell extracts from fibroblast cell populations and 143B OS cells were prepared using a lysis buffer RIPA (Radio Immuno Precipitation Assay buffer), containing 150 mM NaCl, 1% Triton X-100 (X-100-500ML, Sigma-Aldrich), 0.5% sodium deoxycholate (D6750, Siga-Aldrich), 0.1% SDS (161-0301, BioRad), 50 mM Tris (T1378, Sigma-Aldrich) (pH=8) and 2 mM EDTA (EDS-100G, Sigma-Aldrich) and a mixture of proteases and phosphatases (04906845001, Roche) inhibitors and 1 mM of dithiotreitol (DTT; D0632, Sigma-Aldrich) during 30 min at 4º C. After incubation, the samples were sonicated using an ultrasound device (Vibra cell Sonics and Materials Inc. Danbury, CT, USA), at 40 MHz, with 3-5 pulses for 5 seconds, while dipped in ice.

For protein extraction from lung tissue, lungs were homogenized with RIPA buffer at a ratio of 0.5mL *per* 0,1g tissue by manual solubilization with a glass potter (Wheaton, USA).

After that, the samples were dipped on ice for 1 h with regular vortex mixing, and sonicated at 35-40 MHz, with 3 pulses repeated twice for 30 sec followed by centrifugation at 16 000 g for 15 min at 4°C. The supernatant was collected to a new microcentrifuge tube and the protein quantified.

Protein concentration was determined using the bicinchoninic acid (BCA; Sigma-Aldrich, MO, USA) method with BSA (Sigma-Aldrich, MO, USA) as a standard, in a 96-well cell culture plate. In this method, complexes of protein and Cu^{2+} in alkaline conditions are formed, followed by the reduction of Cu^{2+} to Cu^{+}. This reduction is proportional to the amount of protein present in the well. To perform this assay, a standard curve with increasing concentrations of BSA (0 up to 2000 µg/mL) per well was made. The samples were diluted 5x or 50x in H_2O mQ and added to each well 200 µL of a combined reagent of copper sulfate and 50 volumes of bicinchoninic acid. This reagent was incubated for 30 min at 37°C. After this period, the absorbance was read at a wavelength of 570nm in an ELISA microplate reader (BioTek Sinergy HT, LabX, Canada).

Next, the protein samples were denatured using a 4x denaturing solution [0.25 M Tris (pH 6.8; Sigma-Aldrich, MO, USA), 200 mM DTT, 4% (w/v) SDS, 20% (v/v) glycerol (Sigma-Aldrich, MO, USA) and bromophenol blue], in a dilution of 1:4. The samples were heated at 95°C for 5 min and stored at -20°C until use.

Sodium Dodecyl Sulphate Polyacrylamide Gel Electrophoresis (SDS-PAGE) and Electrotransference

Samples with 20-50 µg of protein were loaded into SDS-polyacrylamide gels [8% and 12% acrylamide/bisacrylamide solution (VWR, Ohio, USA), 20% SDS, 10% ammonium persulfate (APS; AMRESCO, USA) and tetramethylethylenediamine (TEMED; Sigma-Aldrich, MO, USA)] and proteins were separated considering their molecular weight by electrophoresis for 10 min at 100 V followed by 1 h at 140 V in buffer solution [100 mM Tris-HCl containing 100 mM bicine (Sigma-Aldrich, MO, USA) and 0.1% (w/v) SDS], using a Bio-Rad Mini-Protean Electrophoresis system. A protein marker (2.5 µL; GRS Protein Marker Multicolour (Grisp, Porto, Portugal) was also used in electrophoresis to estimate the molecular weight of the proteins of interest. After electrophoresis, proteins were transferred from the polyacrylamide gel to a methanol-activated hydrophobic polyvinylidene difluoride (PVDF) membrane. The electrotransference was performed in electrotransfer buffer solution [12.5 mM Tris-HCl (pH 8.0-8.5) containing 96 mM glycine (Sigma-Aldrich, MO, USA) and 20% (v/v) methanol (VWR International, PA, USA)] during 2 h at 0.3 A and 4°C.

Immunoblotting and quantification

After transference, the membranes were blocked in 1% or 5% (w/v) BSA (Sigma-Aldrich, MO, USA) or 5% (w/v) nonfat dry milk in tris-buffered solution T [TBS-T; 20 mM Tris (pH 7.6) and 137 mM NaCl, containing 0.1% (v/v) Tween 20 (VWR International, PA, USA)] for 1 h at room temperature, with soft agitation. This step is

essential to prevent non-specific interactions between the membrane and the antibody used for detection and reduce the background.

After blocking, membranes were incubated overnight at 4°C with primary antibodies or 1h at RT at appropriate dilutions in 1% or 5% (w/v) BSA or 5% (w/v) nonfat dry milk in TBS-T according to the antibody's datasheet.

On the following day, membranes were washed three times for 10 min in TBS-T with soft agitation and then incubated for 1 h at room temperature with the appropriate secondary antibody (Immun-Star Goat Anti-Mouse (GAM)-HRP Conjugate, 170-5047, BioRad; ImmunStar Goat Anti-Rabbit (GAR)-HRP Conjugate, 170-5046, BioRad). Membranes were washed again three times for 10 min, incubated with ECL reagent (Clarity Western ECL Substrate, BioRad), and revealed using ImageQuant LAS 500 (GE Healthcare, USA).

All membranes were incubated with a loading control to further quantified the expression levels of the protein of interest. For that, α-tubulin was used as loading control to the lung tissue samples, and β-actin for fibroblasts and 143B OS cells incubated with the NFs, $NAFs^{SCR}$ and $NAFs^{SCT}$-derived secretome.

Protein quantification was performed using Image J software. Band intensity of target proteins was normalized to their corresponding β-actin and α-tubulin controls.
The details of antibodies used in Western blotting are summarized in Table 2.2.

Table 2.2 - Parameters used in Western Blot.

Protein	Molecular Weight (kDa)	Blocking Solution (In TBS-T)	Primary Antibody Dilution	Primary Antibody Incubation	Secondary Antibody (1:10000)
α-SMA	42	5% BSA	1:1000	1h, RT	Anti-Rabbit
Fibronectin	262	1% BSA	1:500	Overnight, 4°C	Anti-Rabbit
β-catenin	92	1% BSA	1:1000	Overnight, 4°C	Anti-Mouse
pERK	42, 44	5% BSA	1:2000	Overnight, 4°C	Anti-Rabbit
p-p38	43	5% BSA	1:1000	Overnight, 4°C	Anti-Rabbit
Integrin β1	115, 135	5% BSA	1:1000	Overnight, 4°C	Anti-Rabbit
TGF-βRII	65	5% BSA	1:1000	Overnight, 4°C	Anti-Rabbit
α-tubulin	50	5% Milk	1:1000	Overnight, 4°C	Anti-Mouse
β-actin	45	5% Milk	1:1000	1h, RT	Anti-Mouse

2.12 Fibronectin cell adhesion assay

We performed an adhesion assay to test cell adhesion of 143B cells to fibronectin, which is an adhesive extracellular matrix protein commonly found in the lung parenchyma. The 143B cells were exposed to the fibroblasts-derived secretome for 48h and 72h and then plated in a 96-well plate ($2x10^4$ cells/well) previously coated with 10 μg/mL of fibronectin (Sigma-Aldrich, MO, USA) or with 1% BSA (Sigma-Aldrich, MO, USA) as negative control. Cells were incubated for 10 min at 37°C in a humidified atmosphere of 5% CO_2 to allow cell adhesion. After this period, the culture medium was removed, and the wells washed with PBS containing 1 M $CaCl_2 \cdot 2\ H_2O$ and $MgCl_2 \cdot 6\ H_2O$ to remove non-adherent cells.

As the 143B cells express the luciferase gene reporter, the percentage of attached viable cells to the bottom of the plate was estimated based on the bioluminescent signaling emitted. For that, after the last wash, 100 μL EMEM culture medium containing 0.3 mg/mL of D-luciferin was added to each well, and the plate was read in a IVIS Lumina optical imaging system. The bioluminescent signal was measured quantitatively and expressed in photons/second through Living Image 4.10 (Xenogen, Alameda, CA, USA).

To block integrin β1, untreated and secretome-treated 143B cells were incubated with a well-established integrin β1 blocking antibody, the clone P5D2 (10 μg/mL; MAB17781, R&D systems, USA) for 30 min at 37 °C before the initiation of the adhesion assay.

2.13 Cell chemosensitivity analysis - Resazurin assay

The chemosensitivity of 143B cells to doxorubicin was analyzed using the resazurin-based viability assay. Cells were pre-incubated with the fibroblasts-derived secretome for 72h and then plated in a 96-well plate at density of 3500 cells/well. Next day, cells were incubated with increasing concentrations of Doxorubicin (DOXO-cell, STADA) ranging from 0.25 μM to 50 μM for 48h. Non-exposed 143B cells to fibroblasts-derived secretome were treated with the same drug concentrations. Cell viability was

assessed using a resazurin assay that measures the mitochondrial metabolic activity in viable cells. For this purpose, 50 µM of resazurin (Sigma-Aldrich, MO, USA) was added to each well and incubated during 4h at 37°C in 5% CO_2 protected from light. The absorbance was read at a wavelength of 570nm with a reference filter of 600nm in an ELISA microplate reader (BioTek Sinergy HT, LabX, Canada). Absorbance values were normalized to the untreated control cells. Concentration-effects curves were generated, and the half-maximal inhibitory concentration (IC_{50}) was calculated via a non-linear regression analysis.

2.14 Statistical analysis

All results are expressed as mean ± standard error of the mean (SEM). Data were analyzed using the multiple level analysis of variance (ANOVA) followed by a non-parametric Kruskal-Wallis test for multiple comparisons using GraphPad Prism Software version (GraphPad Software, San Diego, CA, USA). Values were considered to statistically significant if $P < 0.05$.

3. Results

3.1 143B OS cells-derived secretome induces ECM remodeling in the lung tissue

In OS, the lung tissue is the most common site for metastatic formation[60]. As previously mentioned, the PMN is a favorable microenvironment that supports and facilitates the proliferation and colonization of cancer cells which is prepared by the primary tumor through the release of several soluble factors and EVs, including exosomes[33].

To access the effects of the OS primary tumor-derived secretome in the lung tissue before the development of metastasis, three mice groups were used. The first group was composed of untreated animals (control). In the second group, mice were treated with the 143B OS cells-derived secretome, and in the third, animals were implanted subcutaneously with 143B OS cells. Both approaches were used to see if the administration of 143B-cells derived secretome can mimic the lung alterations induced by primary tumor-secreted bioactive factors. At the end of the secretome treatment or after tumors reaching a diameter of 5-7 mm, mice were euthanized, and their lungs were harvested and histologically examined to evaluate the EMC remodeling in terms of collagen and fibronectin expression (Figure 3.1 A).

The IHC analysis revealed an increased deposition of reticulin fibers (collagen type I/III) and fibronectin in the lung tissue derived from both experimental groups compared to healthy lungs. These alterations in the collagen and fibronectin expression suggest a dysregulation of the ECM remodeling of the lung microenvironment that might foster cancer cells adaptation and proliferation.

The levels of fibronectin were also evaluated by western blot. Accordingly, the results showed a significant increase (*P<0.05) of fibronectin in the lungs from mice bearing a primary tumor compared with those of untreated mice. Moreover, a trend to

an increased expression of fibronectin in animals treated with the 143B OS cells-derived secretome was also observed compared to the control group (Figure 3.1 B and C).

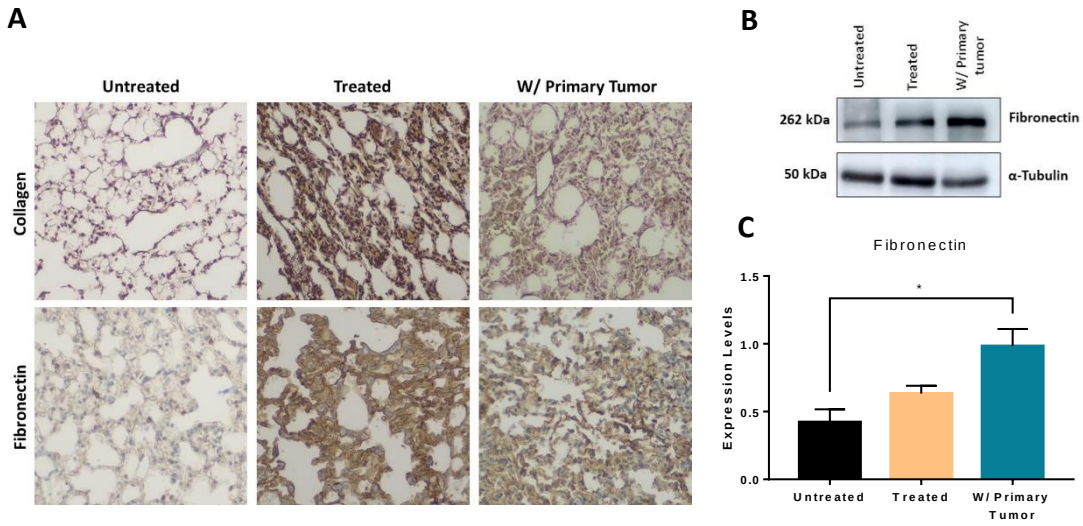

Figure 3.1 – Characterization of the lung tissue from untreated mice, treated with 143B OS cells secretome or bearing a subcutaneous primary tumor. (A) Representative images of the IHC stained lung sections of reticulin fibers (collagen type I/III) and fibronectin (magnification 200x). (B) Representative western blot for fibronectin in lung tissue of the three mice groups with the respective β-actin levels. (C) Relative fibronectin levels in lung extracts from untreated, treated, and mice bearing a primary tumor, normalized to β-actin. Results are presented as ± SEM (n=3). **P*<0.05 when compared to the lungs from untreated mice using a one-way ANOVA with a Kruskal-Wallis test for multiple comparisons.

It is well known that several bioactive factors, including growth factors, inflammatory cytokines, chemokines, interleukins are present in the cancer cells-derived secretome that can induce a pro-inflammatory and pro-angiogenic phenotype in the metastatic site[56].

Considering this, we evaluated the relative mRNA expression levels of some cytokines (TGF-β, IL-1β, IL-6, and TNF-α) in the lung tissue harvested from the three groups of animals (Figure 3.2).

Data analysis showed a trend towards upregulation of TGF-β and a marked decrease of the pro-inflammatory cytokine IL-1β either in secretome-treated animals or carrying a primary tumor (**P*<0.05, ***P*<0.01) as compared with the control group.

TNF-α was also found to be up-regulated but only with statistical significance in the secretome-treated group versus control (*P<0.05). No significant differences were observed in IL-6 relative mRNA expression values between groups.

TGF-β is an immunosuppressive cytokine known to play a critical role in the TME by promoting tumor cells proliferation, differentiation, and invasion, which could explain its upregulation in the lung tissue of mice primed with the secretome or carrying a primary tumor, as well as the suppression of the pro-inflammatory IL-1β cytokine that was observed. TNF-α is a positive regulator of angiogenesis and vascular permeability which could favor the seeding of tumor cells in the lung.

Overall, these data confirmed the establishment of an inflammatory environment during lung PMN formation.

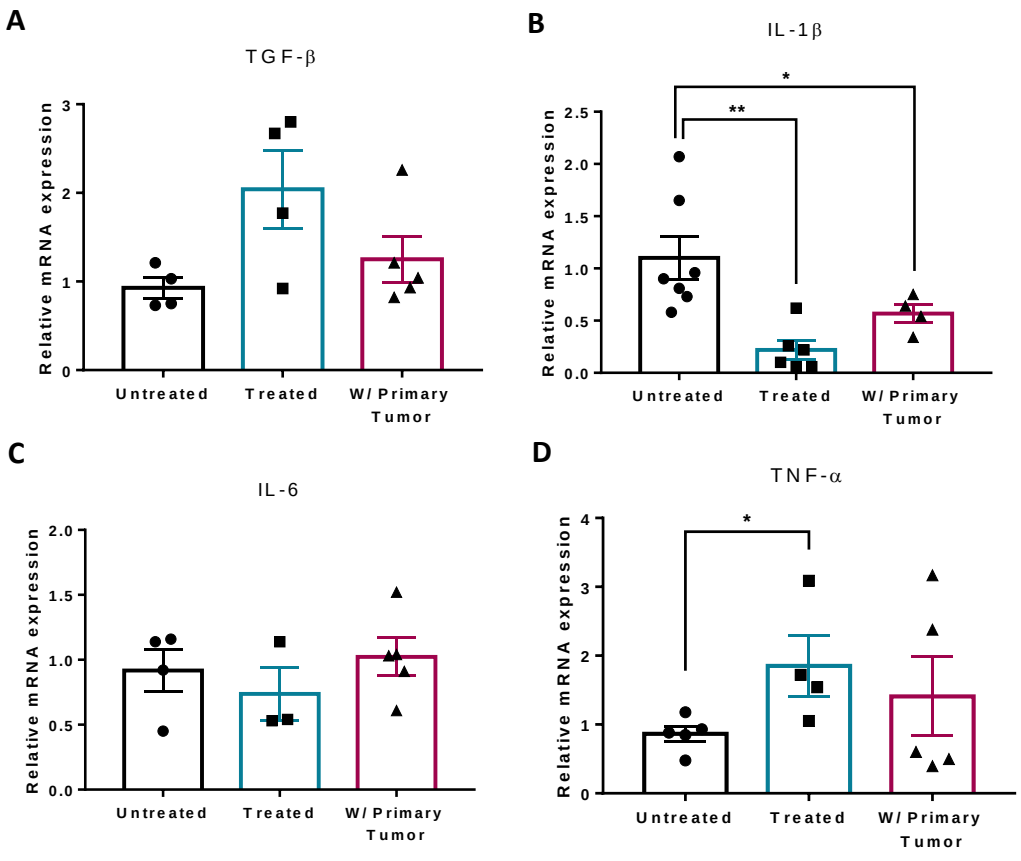

Figure 3.2 – qRT-PCR analysis of inflammatory cytokines in lung tissue from untreated mice, treated with the 143B OS cells derived secretome or bearing a subcutaneous tumor. Relative mRNA expression of TGF-β (A), IL-1β (B), IL-6 (C), and TNF-α (D) of lungs treated with the secretome or carrying a primary tumor in comparison with untreated mice. Values were calculated based on normalized Ct values

relative to lung tissue derived from untreated mice using two housekeeping genes, GAPDH and HPRT-1. The results are presented as mean ± SEM (n=3-7). *P<0.05 and **P<0.01 significantly different when compared with lung tissue derived from untreated mice values using Mann-Whitney tests (t tests).

3.2 143B cells-derived secretome or the presence of a subcutaneous tumor induce an activated-like phenotype in lung fibroblasts

Fibroblasts are one of the most abundant stromal cells in the pulmonary interstitium, being recognized as important players in PMN formation. Therefore, we evaluated the activation state of fibroblasts during the PMN formation.

Fibroblasts were isolated from lung tissue harvested from treated mice or bearing a primary tumor and from control mice and assayed by immunofluorescence for common markers of fibroblasts activation: α-SMA, vimentin, and fibronectin.

The immunostaining and the fluorescence intensity quantifications (Figure 3.3 A and B) showed a significant increase in the α-SMA, a marker of contractility alongside vimentin, also involved in cell motility in fibroblasts isolated from either treated mice or those with a primary tumor (****P<0.0001). Additionally, the extracellular matrix protein, fibronectin, was also found to be upregulated in these activated fibroblast populations compared with normal fibroblasts (****P<0.0001).

The staining with phalloidin, a marker of F-actin filaments, also revealed a change in the morphology of activated fibroblast compared to the control. These fibroblasts appear to lose their homogeneous elongated morphology towards a more heterogeneous and disorganized structure with irregular shapes. Overall, these findings confirm the acquisition of an activation-like phenotype of lung fibroblasts in secretome-treated mice or carrying a primary tumor.

As a result, fibroblasts from control mice were designed as normal fibroblasts (NFs), while those from treated mice or carrying a primary tumor were designed as normal-activated fibroblasts and identified as $NAFs^{SCR}$ or $NAFs^{SCT}$, respectively.

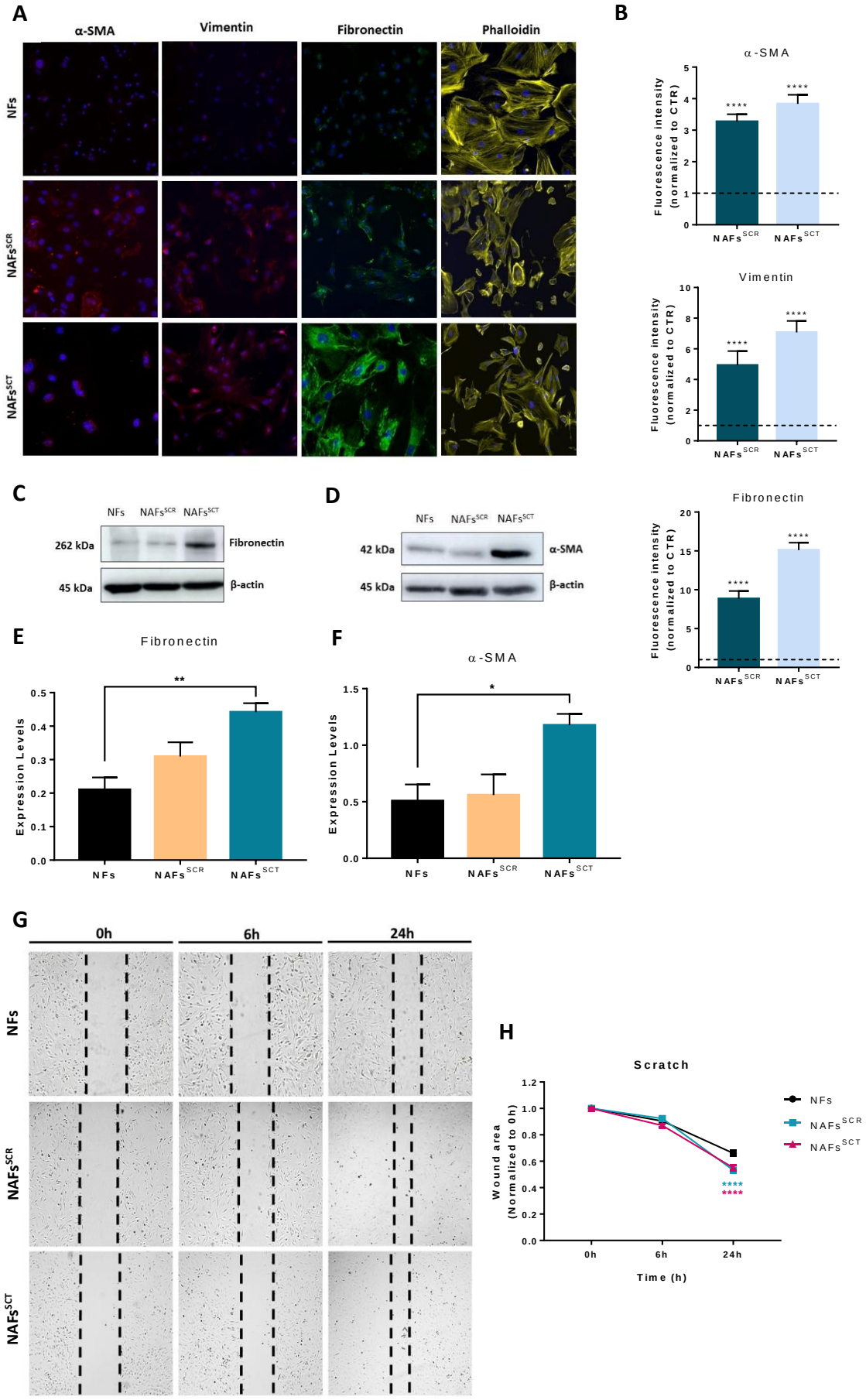
A
α-SMA
Vimentin
Fibronectin
Phalloidin
NFs
NAFs^SCR
NAFs^SCT
B
α-SMA
Vimentin
Fibronectin
Fluorescence intensity (normalized to CTR)
NAFs^SCR
NAFs^SCT
C
NFs
NAFs^SCR
NAFs^SCT
262 kDa
Fibronectin
45 kDa
β-actin
D
42 kDa
α-SMA
E
Fibronectin
Expression Levels
F
α-SMA
G
0h
6h
24h
H
Scratch
Wound area (Normalized to 0h)
Time (h)

Figure 3.3 – Effects of OS cells secretome or a primary tumor on lung fibroblast activation. Representative immunofluorescence images for α-SMA, vimentin, fibronectin, and phalloidin (magnification 20x) and (B) respective fluorescence intensity quantifications. Results are shown as mean ± SEM with ****p<0.0001 significantly different compared with NFs using a one-way ANOVA with a Kruskal-Wallis test for multiple comparisons. Representative western blots for fibronectin (C) and α-SMA (E) in normal and activated fibroblasts and respective quantification (D, F). (G) Representative microscope images of wound areas in fibroblasts at 0h, 6h, and 24h. (H) Graphic representation of relative wound healing area. The scratch area at time-point 0h was set to 1. All results are shown as mean ± SEM with *p<0.05 and **p<0.01 significant differences compared to NFs using a one-way ANOVA with a Kruskal-Wallis test for multiple comparisons for western blot quantification analysis. ****p<0.0001 significantly different compared with NFs wound area at 24h using a one-way ANOVA.

The western blot analysis (Figure 3.3 C, D, E, and F) revealed a significant increase in the fibronectin and α-SMA protein levels in $NAFs^{SCT}$ when compared to NFs (**p<0.01 and *p<0.05, respectively), and a trend for increased fibronectin protein expression in $NAFs^{SCR}$.

Since both α-SMA and vimentin are cytoskeletal proteins important for cell motility, we analyzed the migration ability of the three fibroblast populations by a scratch-wound healing assay during 24h. The results obtained confirmed the increased migratory ability of $NAFs^{SCR}$ and $NAFs^{SCT}$ as compared to NFs (Figure 3.3 G and H), which is another feature of activated fibroblasts.

In addition to producing ECM proteins, fibroblasts within a reactive stroma are also a potential source of inflammatory mediators. In this context, we analyzed the expression of the same cytokines as for the lung tissue in the three fibroblasts populations. The mRNA analysis revealed an expression pattern quite similar to that observed in the lung tissue, except for IL-6, which was upregulated in both activated fibroblast populations (Figure 3.4).

The TGF-β mRNA expression was significantly upregulated (*P<0.05) in $NAFs^{SCR}$ and $NAFs^{SCT}$, as compared with NFs, along with marked downregulation of IL-1β expression that was not even detected in $NAFs^{SCT}$. The expression of TNF-α followed the same tendency observed in the lung tissue with a trend towards an increase in

NAFs^{SCR} and NAFs^{SCT} compared to the control. These results highlight the contribution of fibroblasts to the generation of an inflammatory microenvironment in addition to the ECM remodeling during PMN formation.

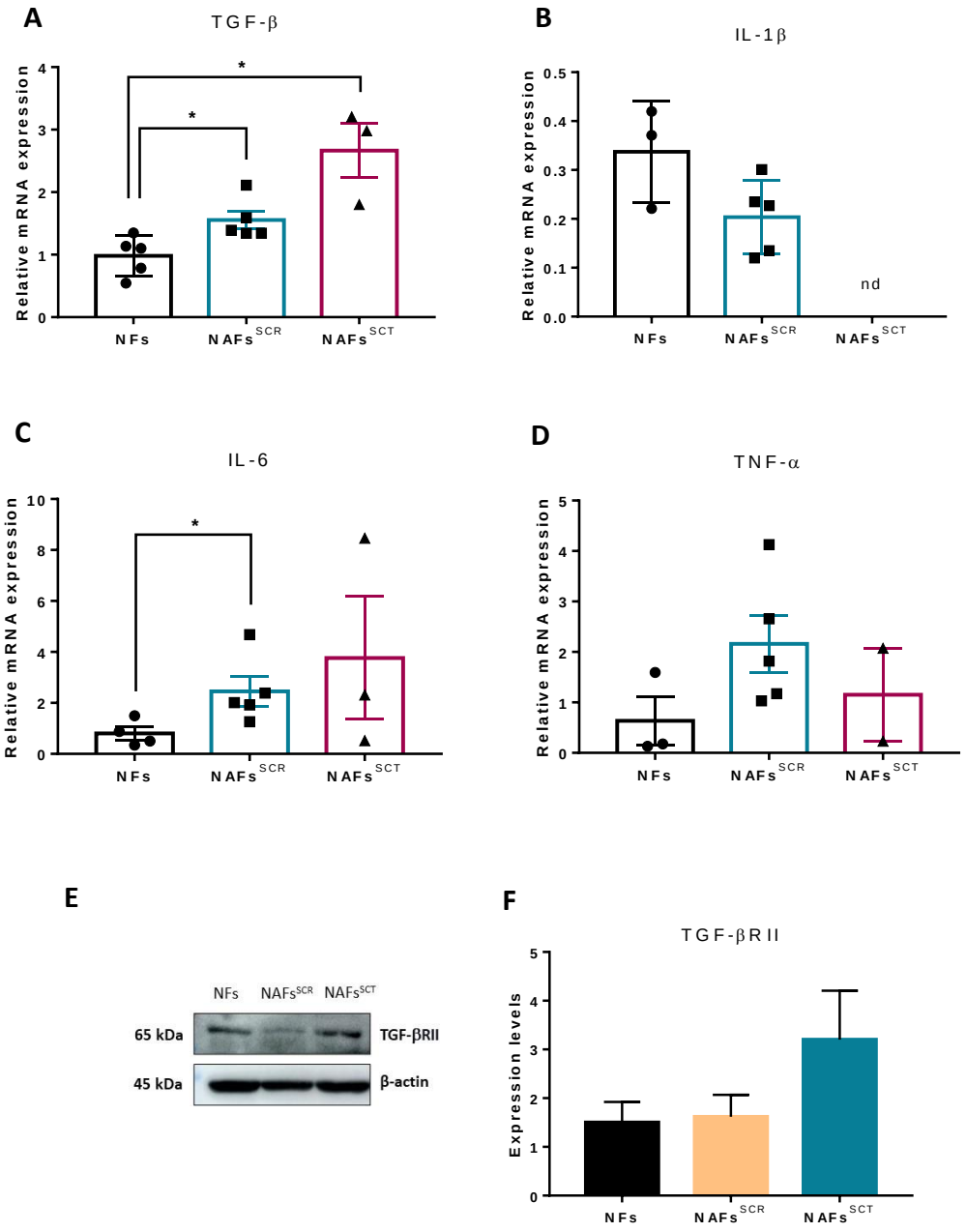

Figure 3.4 – Differential mRNA expression of inflammatory cytokines in normal and activated fibroblasts. Relative mRNA expression levels of TGF-β (A), IL-1β (B), IL-6 (C), and TNF-α (D) in lung fibroblasts from untreated or treated with the secretome or carrying a primary tumor. Values were calculated based on normalized Ct values relative to normal fibroblasts (NFs) using two housekeeping genes, GAPDH and YWHAZ. The results are presented as mean ± SEM (n=3-5). *P<0.05 significantly different when compared with the NFs values using multiple Mann-Whitney tests (t tests). (E)

Representative images and (F) quantification of TGF-βRII expression levels normalized to β-actin expression levels. Results are shown as mean ± SEM (n=3).

TGF-β is a pleiotropic growth factor strongly implicated in tumor progression and metastatic spread in osteosarcoma. This cytokine is a critical regulator of the dynamic stromal alterations that instigate a permissive pre-metastatic niche.

To see if this regulatory cytokine might act in an autocrine manner in fibroblasts, we measured the protein expression levels of TGF-β type II receptor (TGF-βRII) by western blot. The results revealed a trend toward an increase of this receptor in fibroblasts isolated from mice bearing a primary tumor, but not in those derived from mice treated with the secretome, whose levels were in the same range of NFs (Figure 3.4 E and F). Although the increased expression of TGF-βRII in $NAFs^{SCT}$ suggests a contribution of autocrine TGF-β signaling in these cells, other receptors and components of this pathway should be analyzed.

3.3 Activated fibroblasts-derived secretome induces a chemoresistance phenotype in 143B OS cells

Doxorubicin is one of the main compounds of the conventional chemotherapy regimen used in the treatment of OS[24]. We evaluated the chemosensitivity of 143B cells to this chemotherapeutic drug after a 48h-incubation period with different concentrations ranging from 0.01 to 100 μM. Cell viability was analyzed using a resazurin colorimetric assay. The half-maximal inhibitory concentration (IC_{50}) was calculated via a non-linear regression analysis, which was approximately 1 μM (Figure 3.5 A).

To evaluate whether the activated fibroblast-derived secretome could alter the susceptibility of 143B cells to doxorubicin, 143B cells were pre-treated with the NFs, $NAFs^{SCR}$, and $NAFs^{SCT}$-derived secretome for 72h, and then incubated with increasing concentrations of doxorubicin ranging from 0.25 μM to 5 μM (below and above the IC_{50}) for 48h. Non-exposed 143B cells to fibroblasts-derived secretome were treated with the same drug concentrations. The results revealed a significant increase in cell viability in 143B pre-treated with $NAFs^{SCR}$ and $NAFs^{SCT}$-derived secretome as compared

to the non-treated 143B cells (Figure 3.5 B) exposed to the same drug concentrations. This resistance phenotype was observed in all the tested doxorubicin concentrations. No significant differences were observed between untreated 143B cells and those treated with the NFs-derived secretome.

For instance, in cells incubated with the IC_{50} value (1 µM doxorubicin), the increase in cell viability was 20% and 25% when incubated with the secretome of $NAFs^{SCR}$ or $NAFs^{SCT}$, respectively.

Overall, these results suggest that during exposure to the secretome of activated fibroblasts ($NAFs^{SCR}$ and $NAFs^{SCT}$), 143B OS cells activate mechanisms that render them less sensitive to doxorubicin, which might explain their chance to survive chemotherapy and disseminate to form metastasis.

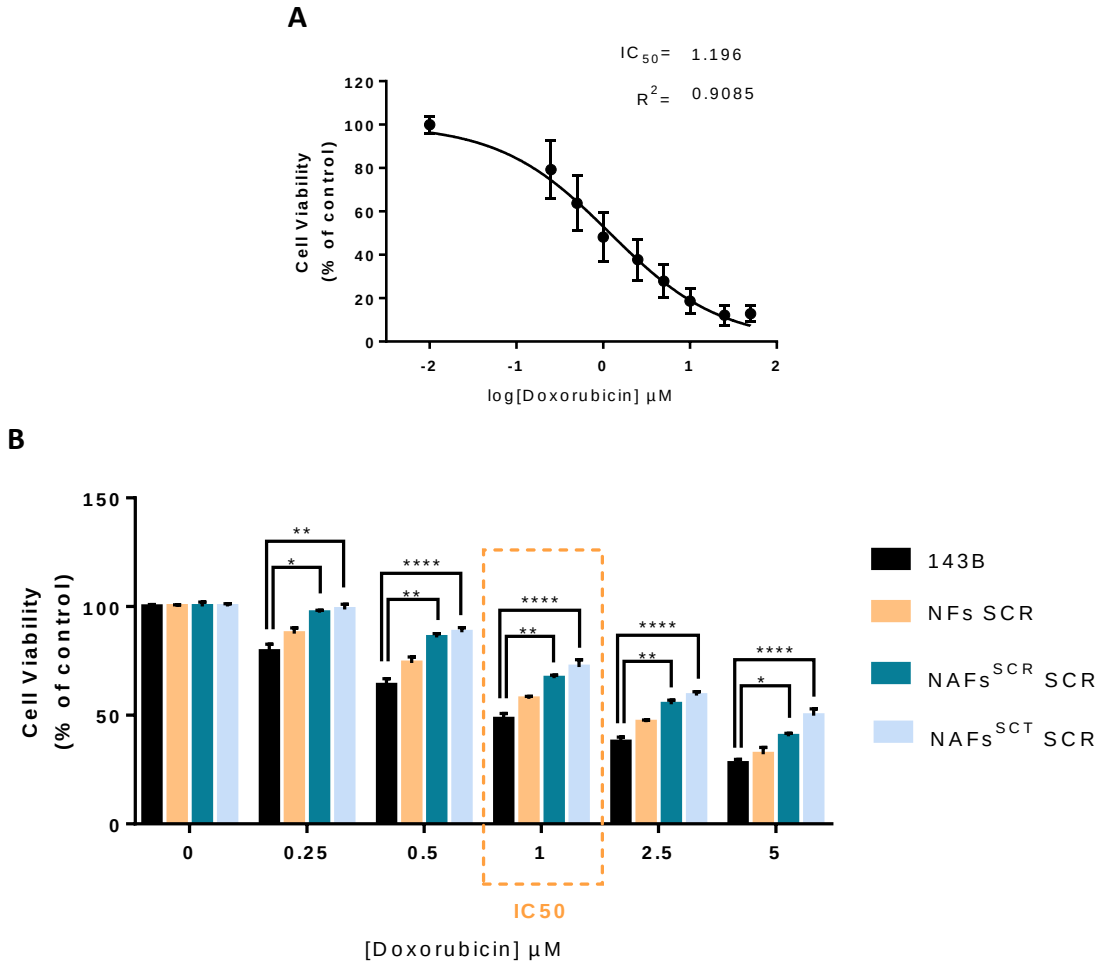

Figure 3.5 - Effects of the activated fibroblasts-derived secretome in the chemosensitivity of 143B cells to doxorubicin. (A) Sigmoidal fitting of the concentration-response curve for DOX IC_{50} calculation. (B)

Effects of the fibroblasts-derived secretome in chemosensitivity of 143B OS cells to DOX. 143B cells were pre-treated with the fibroblasts-derived secretomes for 72h and then incubated with DOX above and below the IC50 value for 48h. *p<0.05, **P<0.01, and ****p<0.0001 significantly different when compared to untreated 143B cells using a one-way ANOVA with a Kruskal-Wallis test for multiple comparisons.

3.4 The 143B cell line contains a stem-like cell population that is exacerbated upon exposure to the secretome of activated fibroblasts

The stemness of cancer cells plays a crucial role in the growth, progression, and survival of tumor cells[114].

The presence of a population of CSCs in the 143B OS cell line was assessed through the ability to form spherical colonies, designed as sarcospheres, when cultured in low-adherent surfaces and serum-free culture medium (Figure 3.6 A). Moreover, the mRNA expression of the pluripotency genes SOX2, KLF4, OCT4, and NANOG was also assessed (Figure 3.6 B). These results revealed a marked expression of the four pluripotency genes compared to parental 143B cells (**P<0.01 and ***P<0.001), which confirms the stemness nature of the isolated sarcospheres. Based on these observations we conclude that 143B cells contain subset of stem-like cells which can be isolated using a sphere-forming assay.

We know from previous reports from our group, the Wnt/β-catenin signaling pathway is activated and regulates the self-renewal of osteosarcoma CSCs[102]. We analyzed the relative mRNA expression of the Wnt ligand receptors, LRP5 and LRP6, and of the target genes, AXIN2 and DKK-1 (Figure 3.6 C). This analysis showed an increased expression of both Wnt ligand-receptors and the signaling target gene, AXIN2 (*P<0.05) as well as a decreased expression of the antagonist DKK-1 (*P<0.05), confirming the activation of the Wnt signaling pathway in 143B-derived spheres.

Next, we evaluated whether the secretome of activated fibroblasts would exacerbate the stemness features of the 143B cells, using the sphere-forming assay as a readout. This assay was performed after a 72h incubation period with the secretome. At the end of the experiment, on the ninth day of culture (Figure 3.6 D and E), the sphere forming efficiency and the spheres' diameter were determined. The results revealed a significant increase in the diameter of spheres derived from 143B cells treated with $NAFs^{SCR}$ and $NAFs^{SCT}$ secretome (****p<0.0001 and ***p<0.001, respectively) compared to the untreated 143B-derived spheres, as well as a trend towards increased sphere-forming efficiency (Figure 3.6 F). Moreover, the mRNA expression analysis showed an upregulation of at least one of the pluripotency-associated transcription factors SOX2 or KLF4 in pre-treated 143B cells with the secretome of activated fibroblasts (Figure 3.6), which plays an important role in reprograming of differentiated cancer cells into CSCs. No significant differences were observed between untreated 143B cells-derived spheres and those treated with the NFs-derived secretome.

Overall, these data showed that the secretome from activated fibroblasts promotes an enrichment in the stemness properties of the 143B cells. These might explain the increased chemoresistance of secretome-treated cells to doxorubicin.

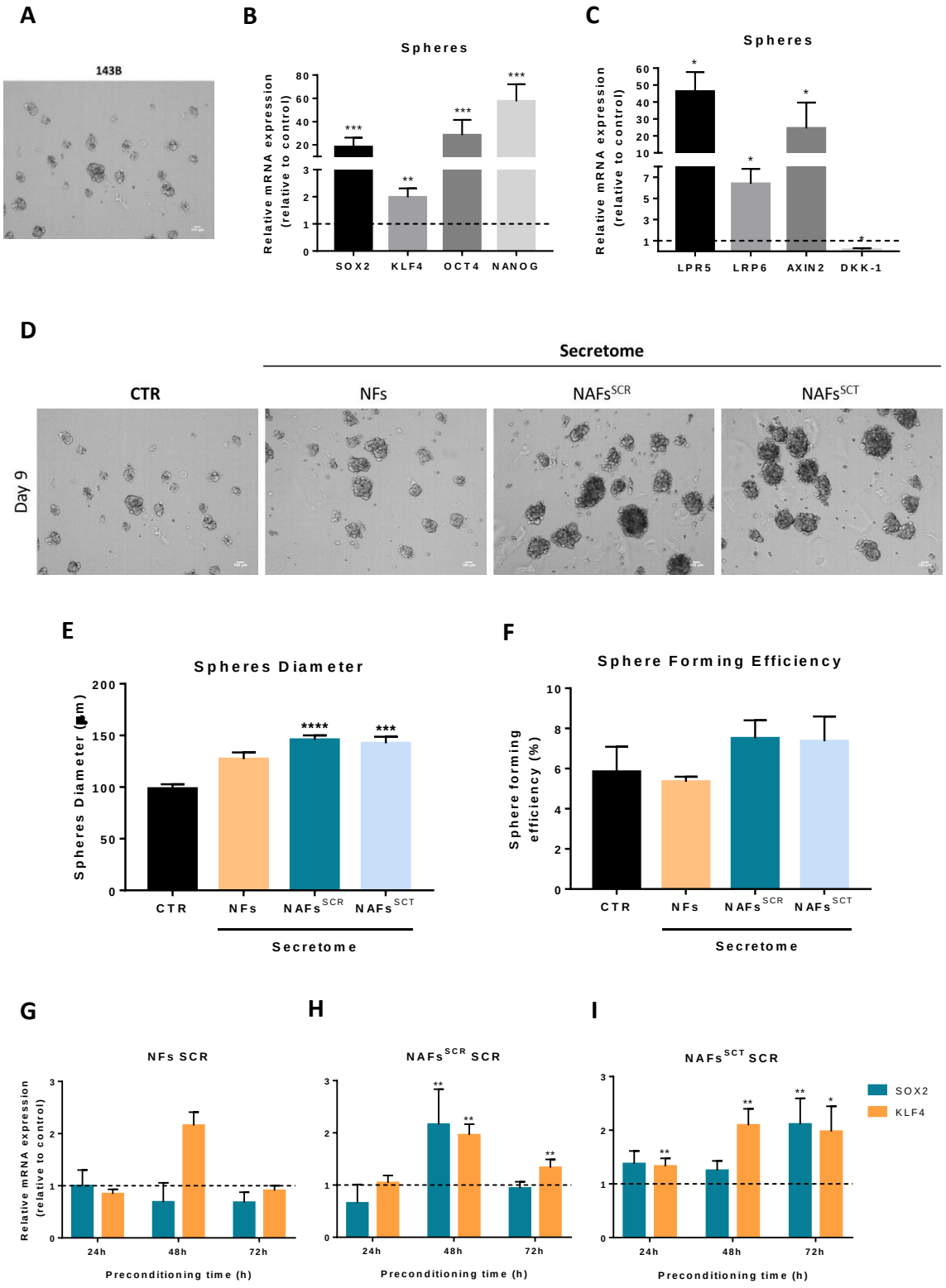

Figure 3.6 – Evaluation of the presence of a subpopulation of CSCs in the 143B OS cells culture and assessment of the effects of the fibroblasts-derived secretome in the induction of stem-like properties in 143B cells. (A) Representative image of spherical colonies derived from the 143B OS cell line in serum-free medium. (B) Relative mRNA expression of the pluripotency genes, SOX2, KLF4, OCT4 and

NANOG, and (C) the Wnt/β-catenin signaling pathway activation markers, LRP5, LRP6, AXIN2, and DKK-1. Values were calculated based on normalized Ct values relative to control, 143B OS cells, using two housekeeping genes, GAPDH and HPRT-1. Results are presented as mean ± SEM (n=3). *p<0.05, **p<0.01, and ***p<0.001 significantly different when compared with 143B cells relative mRNA expression using multiple Mann-Whitney tests (t tests). (D) Representative images of the size and number of the spheres derived from parental and fibroblasts secretome-treated 143B cells (magnification 40x). The 143B cells were incubated with NFs, $NAFs^{SCR}$, and $NAFs^{SCT}$-derived secretome for 72h. (E) Spheres diameter (μm) and (F) sphere forming efficiency as a percentage of formed spheres. The results are shown as mean ± SEM (n=3-9). ***p<0.001 and ****p<0.0001 significantly different compared with the control using a one-way ANOVA with a Kruskal-Wallis test for multiple comparisons. Relative mRNA expression of the pluripotency genes, SOX2 and KLF4, in 143B OS cells incubated with the fibroblasts-derived secretomes for (G) 24h, (H) 48h, and (I) 72h. The relative mRNA expression values were calculated based on normalized Ct values relative to control, 143B OS cells, using two housekeeping genes, GAPDH and HPRT-1. The results are presented as mean ± SEM (n=3). *p<0.05 and **p<0.01 significantly different compared to 143B OS cells using multiple Mann-Whitney tests (t tests).

To see if this enrichment in stem-like cells is mediated by the Wnt pathway activation, we analyzed the mRNA expression of Wnt ligand receptors, LRP5 and LRP6, and the Wnt target gene AXIN2 in 143B treated cells with the secretome of activated fibroblasts (Figure 3.7 A, B, and C). The results showed a modest increase of some these Wnt-related markers, with only LRP6 and AXIN2 expression (*P<0.05) reaching significance in 143B cells incubated with $NAFs^{SCR}$-derived secretome.

We also performed an immunostaining of β-catenin in secretome-treated 143B cells (Figure 3.7 D, E, F and G). In control cells, β-catenin localizes predominantly at cytoplasmic membrane, whereas in treated cells it was observed an accumulation in the cytoplasm, but not in the nuclear fraction, confirmed by a single cell track plot analysis. The western blot analysis revealed similar levels of β-catenin expression in 143B cells amongst the different conditions (Figure 3.7 H and I). Although, we did not observe a degradation of β-catenin, the mixed pattern of membranous and cytoplasmic β-catenin localization is insufficient to determine the Wnt pathway activation status in treated cells.

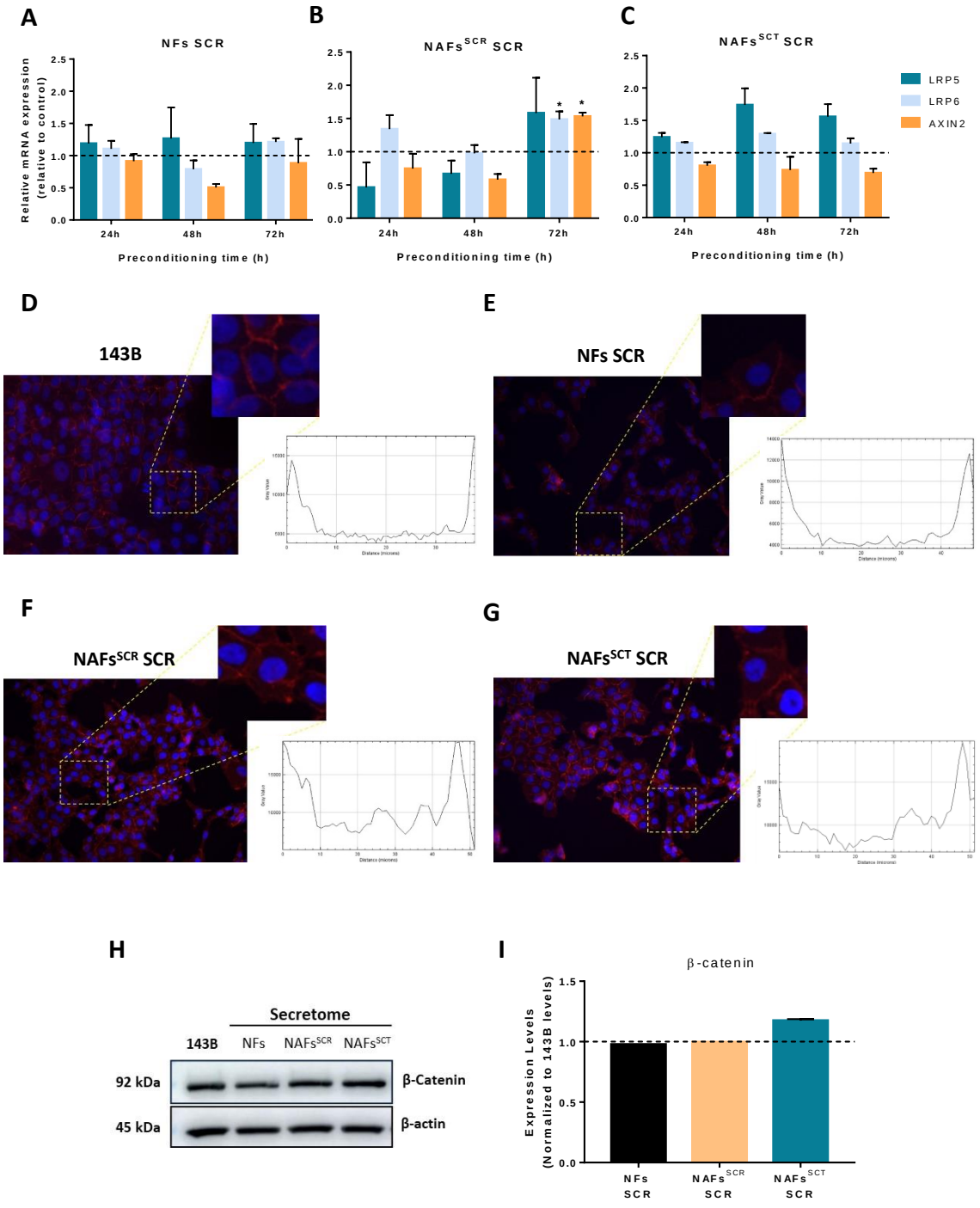

Figure 3.7 - Effects of reactive fibroblasts-derived secretome in the activation of the Wnt/β-catenin signaling pathway in 143B cells. Relative mRNA expression of the Wnt/β-catenin signaling pathway target genes, LRP5, LRP6, and AXIN2, in 143B OS cells incubated with (A) NFs, (B) NAFs^{SCR}, and (C) NAFs^{SCT}-derived secretome. 143B cells were incubated with the fibroblasts secretome for 24h, 48h, and 72h. Relative mRNA expression values were calculated based on normalized Ct values relative to control using two housekeeping genes, GAPDH and HPRT-1. All results are presented as mean ± SEM (n=3). *p<0.05 significantly different compared to 143B cells using multiple Mann-Whitney tests (t tests).

Representative images of β-catenin accumulation in the 143B cells cytoplasm (D) untreated and pre-treated with the (E) NFs, (F) $NAFs^{SCR}$, and (G) $NAFs^{SCT}$-derived secretome for 72h (magnification 20x) with a single cell track plot analysis for the location of β-catenin. (H) Representative western blot images of β-catenin and β-actin levels with the quantification of the β-catenin expression levels relative to β-actin loading control. 143B cells were incubated with the fibroblasts-derived secretome for 48h (I). The results are normalized to the control, the untreated 143B cells. All results are shown as mean ± SEM (n=1-2).

3.5 Effect of activated fibroblasts in 143B OS cells entry into a dormant-like state

In the adaptation process to the new microenvironment, disseminated cancer cells may enter in a non- or slow-proliferative dormant state, in which they remain viable but stop proliferating, thus being undetected with the current diagnosis methods[144]. Dormant cells are characterized by increased p38 MAPK and decrease ERK activity. Thus, cells with $ERK^{high}/p38^{low}$ activity are highly proliferative, whereas those with $ERK^{low}/p38^{high}$ activity are in dormancy[164].

Based on this, we evaluated the influence of activated fibroblast-derived secretome on 143B cells fate by determining the pERK/p-p38 activity ratios at various incubations time points.

The 143B cells were treated with the NFs, $NAFs^{SCR}$, and $NAFs^{SCT}$-derived secretome for 24h, 48h, and 72h. The expression levels of the pERK and p-p38 were evaluated by western blot and normalized to their correspondent β-actin levels. The ratio pERK/p-p38 was determined for each condition (Figure 3.8).

The basal ERK to p38 MAPK ratio in 143B cells was 1.53, predictive of a proliferative phenotype. When incubated with NFs-derived secretome, the ERK/p38 activity ratio decreased slightly due to an increase in the phosphorylation of p38 but remained above 1.

In treated 143B cells with the secretome of activated fibroblasts, the protein levels of phosphorylated p38 at 24h increase, resulting in a $pERK^{low}/p\text{-}p38^{high}$ ratio (<1), indicating that cells are entering into a slow-proliferating or dormant-like condition. Along with the preconditioning time, p38 activity (assessed by its phosphorylation) gradually decreased, and at 72h, the average pERK/p-p38 ratios were higher than 1,

favoring a proliferative state. Apparently, multiple secreted factors by activated fibroblasts converge to drive dormancy in tumor cells through activation of p38 signaling, which appears to decrease over time, while maintaining the constitutive ERK activation.

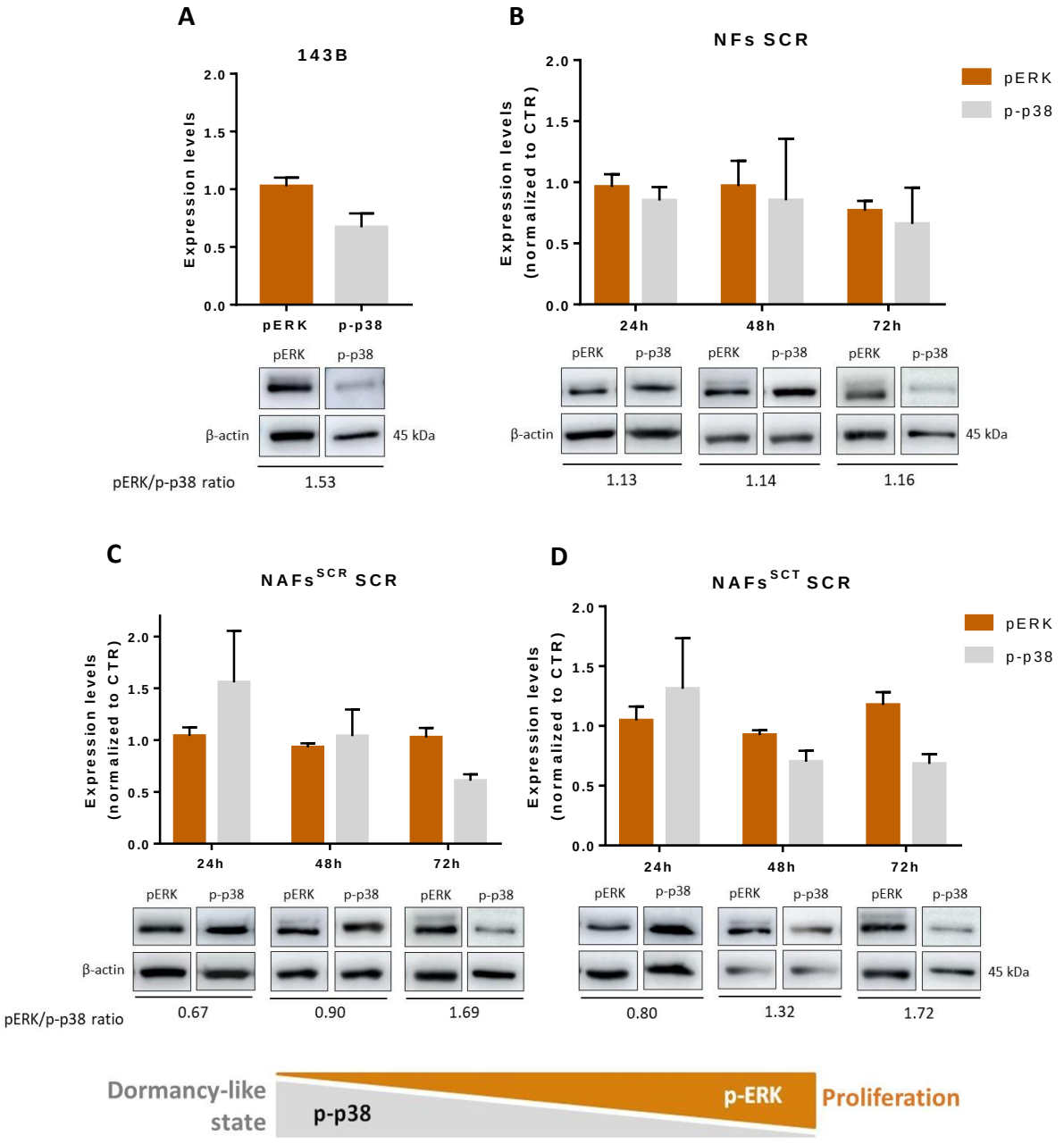

Figure 3.8 - Analysis of ERK and p38 MAPKs activities in 143B cells during exposure to fibroblasts-derived secretome. Representative western blots images and quantification of pERK (42, 44 kDa) and p-p38 (43kDa) levels with the respective β-actin levels in untreated and 143B cells incubated with NFs,

NAFs^{SCR}, and NAFs^{SCT}-derived secretome for 24h, 48h, and 72h, (A) (B), (C), and (D). Quantification of pERK and p-p38 expression levels normalized to the control, untreated 143B cells. Determination of the pERK/p-p38 ratio for all conditions. All results are presented as mean ± SEM (n=3-6).

3.6 Secretome of activated fibroblasts promote the adhesion of 143B cells to fibronectin via integrin β1

The adhesion of disseminated tumor cells to ECM matrix proteins via integrins represents a crucial step in the process of metastization to allow cell survival and colonization at secondary sites[155].

The IHC analysis of lung tissue from animals with a primary tumor or treated with the secretome of 143B showed an increased deposition of fibronectin, which is a ligand for numerous adhesion receptors or integrins, including integrin β1 (Figure 3.1). The expression of this cytokine has been associated with the invasive and metastatic behavior of tumor cells[156].

We analyzed the constitutive expression of this integrin in 143B cells that are described as highly metastatic[165]. The western blot analysis confirmed a marked expression of integrin β1 in these cells, that increased significantly after an incubation period with the secretome of activated fibroblasts NAFs^{SCR} or NAFs^{SCT} (Figure 3.9 A and B) at 48h and 72h. On the other side, incubation with the secretome of NFs had no significant effects on the expression levels of integrin β1 in relation to untreated control cells or between different time points, suggesting that the secreted factors by NFs did not induce any significant changes in OS cells phenotype.

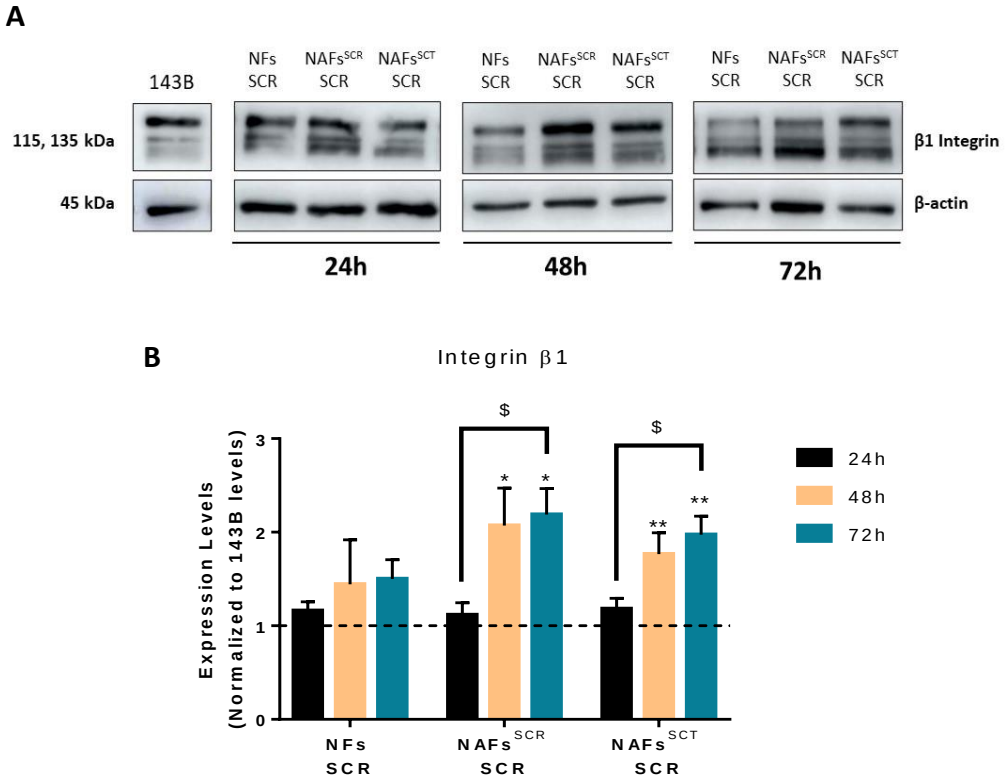

Figure 3.9 – Western blot analysis of Integrin β1 in 143B cells. (A) Representative western blot images of integrin β1 in 143B OS cells before and after incubation with NFs, NAFs^{SCR}, and NAFs^{SCT}-derived secretome for 24h, 48h, and 72h. (B) Graphic representation of the expression levels of integrin β1, normalized to untreated 143B cells. All results are shown as mean ± SEM (n=6). *P<0.05 and **P<0.01 significantly different compared with 143B OS cells using a one-way ANOVA with a Kruskal-Wallis test for multiple comparisons. $$P$<0.05 significantly different compared to 143B cells treated with secretome of NAFs^{SCR} and NAFs^{SCT} with 24h preconditioning using a one-way ANOVA.

To verify whether the increased integrin β1 expression improves the adhesion of 143B cells to fibronectin we performed an adhesion assay using a specific neutralizing antibody to integrin β1.

Preconditioning 143B cells with the secretome of activated fibroblasts increased tumor cells' adhesion to fibronectin as seen in Figure 3.10. NAFs^{SCR} secretome induces a significant increase in the percentage of adhered cells of approximately 60% at 72h pre-incubation (***P<0.001). The adhesion-promoting effects of NAFs^{SCT}-derived secretome were significant as early as 48h by almost 60% and 45% at 72h (**P<0.01 and *P<0.05, respectively).

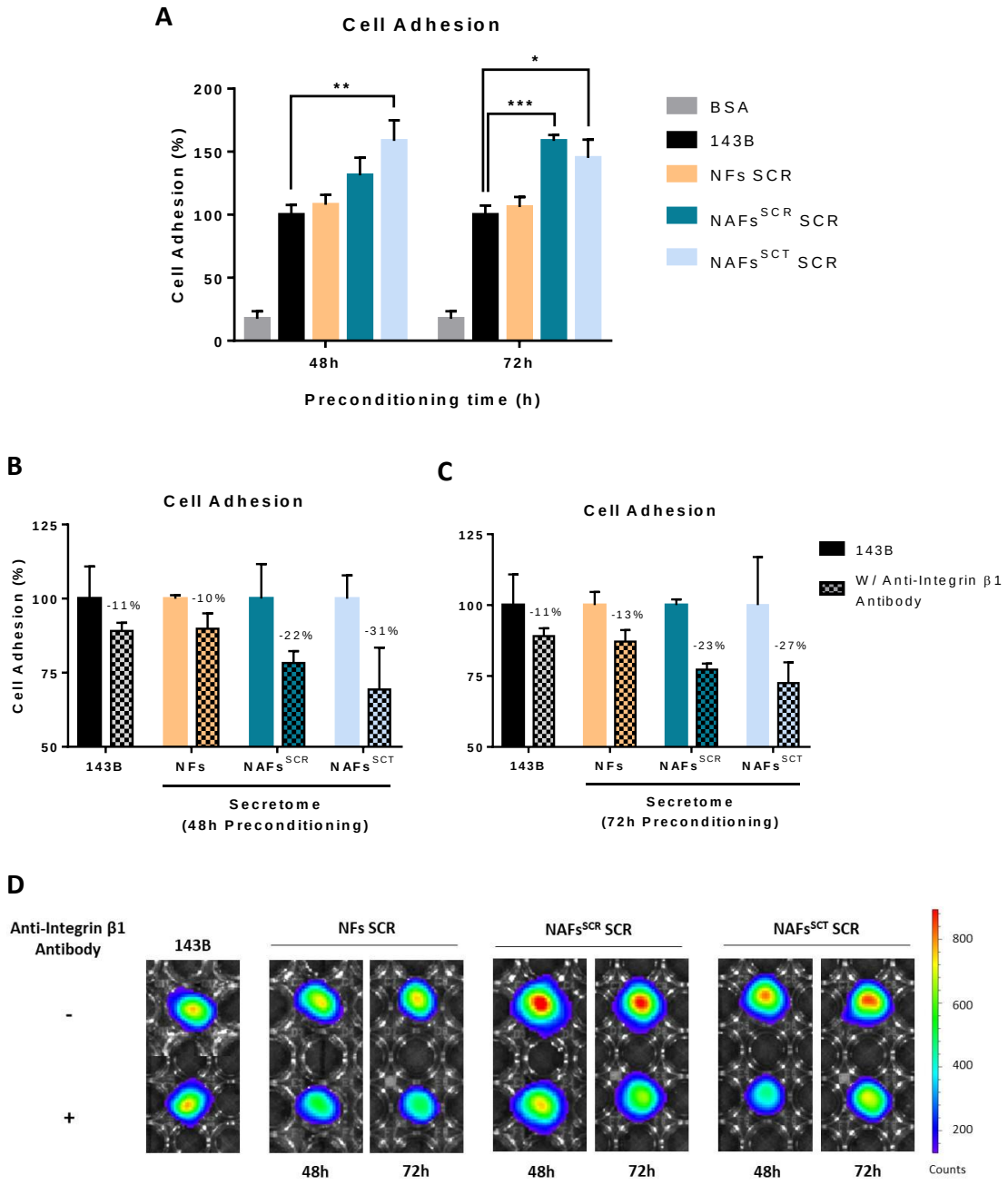

Figure 3.10 – Effects of the activated fibroblasts' secretome on the adhesion of 143B to fibronectin. (A) Adhesion of 143B cells to fibronectin after pre-treatment with NFs, NAFs^{SCR}, and NAFs^{SCT}-derived secretome for 48h and 72h. The adhesion to BSA was used as negative control. All values were normalized to the control, the untreated 143B cells. The results are presented as ± SEM (n=3). *P<0.05, **P<0.01, and ***P<0.001 compared to the untreated 143B cells using multiple Mann-Whitney tests (t tests). (B) and (C) Adhesion assay performed in the presence or absence of a blocking integrin β1 antibody. 143B cells were also incubated with the fibroblasts secretomes for 48h and 72h. All results are showed as ± SEM (n=1). (D) Representative images of the bioluminescent signal of

adhered 143B cells to fibronectin with and without the incubation of the neutralizing integrin β1 antibody.

In the presence of a specific neutralizing anti-integrin β1 antibody, there was a reduction in the adhesion ability of 143B cells to fibronectin, especially for those exposed to the secretome of activated fibroblasts (Figure 3.10 B, C, and D). Neutralizing integrin β1 in control and NFs secretome-treated 143B cells was similar, with a reduction in cell adhesion of approximately 10%. In treated 143B cells with the secretome of $NAFs^{SCR}$ and $NAFs^{SCT}$, blocking integrin β1 antibody resulted in a reduced adhesion to fibronectin by 20 to 30%. Overall, these findings confirm the role of integrin β1 in cells adhesion to fibronectin.

4. Discussion

The metastatic disease remains the principal cause of death for OS patients[35]. About 20-30% of OS patients without metastasis at diagnosis will develop metastasis during the progression of the disease, being the lung the most frequent site of metastatic focus[18,19].

The metastatic formation is a complex process composed of a series of events that start before the dissemination and local invasion of the tumor cells in secondary organs, which begins with the preparation of the PMN[27,28]. Several soluble factors and EVs secreted by the primary tumor modulate this supportive microenvironment promoting suitable conditions for adaptation and further proliferation and colonization of cancer cells in the lungs[29,33]. Characterizing these molecular and cellular alterations that render a distant organ hospitable for disseminating tumor cells is crucial to our understanding of the metastatic process.

With this in mind, this work was intended to unravel the mechanisms by which the primary tumor modulates the lung microenvironment, particularly the stromal fibroblasts, during the PMN formation and how the reciprocal interaction between activated fibroblasts and tumor cells increase their metastatic behavior.

To achieve this goal, we used two different animal models. In the first one, mice were subcutaneously injected with the 143B cells to form a subcutaneous OS primary tumor. The presence of the primary tumor mimics the real condition of patients with OS, wherein the bioactive factors released by the primary tumor will induce the essential changes in the lung microenvironment for further colonization of cancer cells. In the other model, only the secretome of the 143B cells was administered to the animals. Both models revealed similarities in the alterations induced in the lung parenchyma and the subsequent activation of lung fibroblasts. The fact that the secretome-treated model mimics the effects of the presence of a primary tumor reveals the crucial role of the cancer cell secretome as the responsible factor for PMN

formation, confirming the original concept of the PMN appearance with the hypothesis of 'seed and soil' by Stephen Paget in 1889[30].

Lung tissue from both treated animal models displayed increased deposition of reticulin fibers (collagen I/III) and fibronectin. These ECM proteins accumulation in the lung metastatic site have previously been described by others, and they are widely used for adhesion assays to evaluate cancer cells binding to the ECM[166,167].

As the most abundant stromal cells and one of the main focuses of this study, the activation of lung fibroblasts was evaluated. The similarity between the two animal models could still be visible in the alterations promoted to these stromal cells. The fibroblasts derived from mice treated with the 143B secretome or bearing a primary tumor presented increased expression of the activation markers α-SMA, vimentin, and fibronectin. The phalloidin staining also showed a change in the morphology of activated fibroblasts, losing their homogeneous elongated morphology towards a more heterogeneous and disorganized structure with irregular shapes.

The migratory capacity of the activated fibroblasts was also increased, which can be correlated with α-SMA and vimentin expression that, as cytoskeletal proteins, they are crucial for cell motility [168].

Overall, this characterization revealed a modulation of the lung tissue by the accumulation of ECM proteins, including fibronectin and collagen, and the presence of an activated population of lung fibroblasts, based on the increased expression of activation markers and enhanced migratory ability favoring the formation of the PMN. These alterations also suggest a clear involvement of fibroblasts in the PMN formation in the lung orchestrated by tumor-released factors.

As previously mentioned, an inflammatory phenotype is promoted by the release of several cytokines, chemokines, interleukins, and EVs, from the primary tumor[83,89]. Considering this, we evaluated the relative mRNA expression levels of several cytokines, including TGF-β, IL-1β, IL-6, and TNF-α, in the lung tissue as well as in the isolated fibroblasts populations. The mRNA expression levels followed the same pattern in both lung tissue and fibroblasts.

TGF-β is an immunosuppressive cytokine that is known to play a critical role in the TME. This cytokine promotes tumor cells proliferation, differentiation, and invasion. Our data revealed an upregulation of this cytokine in both lung tissue of mice primed with the secretome or carrying a primary tumor. These findings suggest the increased importance of TGF-β in lung tissue remodeling. In other cancer types, such as breast cancer, which also frequently metastasizes to the lungs, IL-1β is considered a crucial interleukin to promote phenotype alterations in the lung. IL-1β increases the accumulation of ECM proteins and allows a new microenvironment formation, prone to the colonization of breast cancer cells[77]. However, in OS, has been shown a suppressive effect of TGF-β towards the IL-1β expression[169], which supports the results obtained. As a positive regulator of angiogenesis and vascular permeability, the increased expression of TNF-α favors the seeding of cancer cells in the lung, also corroborating our results. Additionally, the IL-6 expression, among others, is described as an essential interleukin released by the primary tumor that facilitates glycolytic metabolism in tumor cells, leading to the activation of the MEK/ERK1/2/hypoxia-inducible transcription factor-1α (HIF-1α) pathway[170]. In contrast to the lung results, the fibroblasts analysis revealed a significant increase in the IL-6 expression, suggesting a modulation of the metabolism in tumor cells, culminating in the lung colonization by OS cells.

As a pleiotropic growth factor strongly implicated in tumor progression and metastatic spread in OS, TGF-β might act in an autocrine manner in fibroblasts[171]. TGF-β binds to the high-affinity receptors present in the cellular membrane of fibroblasts, the TGF-βRII, that auto-phosphorylates itself, inducing the formation of a tetrameric complex with the TGF-βRI. Additionally, activated TGF-β receptors promote the activation of the intracellular mediators SMAD2/3 proteins inducing the initiation of a protein phosphorylation cascade, which can regulate TGF-β target gene expression[172].

Through the analysis of the TGF-βRII, we observed that $NAFs^{SCT}$ showed a tendency towards an increase, but not in the $NAFs^{SCR}$ compared to NFs, suggesting that the autocrine TGF-β signaling pathway may be active in $NAFs^{SCT}$, but other components and receptors of this pathway should be further analyzed. The expression of TGF-βRI and the expression of the SMAD 2/3 should be considered.

In sum, the presence of a primary tumor or the 143B cells-derived secretome had similar effects in lung tissue and lung fibroblasts by creating an inflammatory microenvironment, in which TGF-β could be an essential mediator for the appearance of this phenotype.

Fibroblasts as essential components of the lung microenvironment are likely to interact with cancer cells reciprocally. The acquisition of an active phenotype allows fibroblasts to exhibit myofibroblasts characteristics favoring invasive growth and metastasis[65,76,77]. The reciprocal effects of activated fibroblasts on OS cells are not fully understood. This work also aimed to unravel these mechanisms in terms of the induction of cellular resistance to chemotherapy by stem-like characteristics acquisition, the entry of cancer cells into a dormant state, and the increased adhesion of cancer cells to ECM proteins.

The cancer cell resistance to chemotherapy regimens is one of the most known causes for increased mortality in cancer patients[129]. The mechanisms of the acquisition of a resistance phenotype are highly variable depending on the cancer type. In OS, the development of chemoresistance limits the effectiveness of cytotoxic drugs, leading to frequent refractoriness to chemotherapy[128].

In response to doxorubicin, one of the drugs used in the conventional chemotherapeutic regimen[24], the 143B cells incubated with the secretome derived from $NAFs^{SCR}$ and $NAFs^{SCT}$ presented decreased sensibility to doxorubicin, compared to untreated 143B cells. The acquisition of a chemoresistance phenotype can be the result of several mechanisms that enhance their ability to adapt and survive in a hostile environment. For example, CSCs have an effective drug-efflux system, with increased expression of ABC transporters, such as P-glycoprotein[133]. CSCs are described as drivers of metastasis, and metastatic tumors are associated with a more invasive and aggressive cancer phenotype[129]. Additionally, some studies revealed that the expression of stemness markers related to a stem-like phenotype is essential for tumor maintenance being mediators of the cellular resistance [173]. This small population of cells within a tumor can self-renew and generate differentiated cells that constitute a whole tumor[92].

Taking this into account, we assessed the presence of this subpopulation on 143B cells. This highly metastatic OS line has a subset of cells with stem-like properties, isolated by a sphere-forming assay and confirmed by the overexpression of pluripotency genes, SOX2, KLF4, OCT4, and NANOG. Several signaling pathways mediate the acquisition and maintenance of a stem-like phenotype in tumor cells[108,109]. Specifically, the Wnt signaling pathway is described to play a pro-oncogenic role by stimulating cell proliferation and motility, presenting a crucial role in the regulation of CSCs function[116]. Through the analysis of the Wnt ligand receptors LRP5/6, the Wnt target gene, AXIN2, and the antagonist, DKK-1 expressions, we conclude that in spheres derived from 143B cells this signaling pathway is active.

Herein, we observed an exacerbation of the stem-like properties in 143B cells under the exposure to the secretome of activated fibroblasts, confirmed by the upregulation of SOX2 and KLF4 expressions, as well as an increase in the sphere-forming efficiency and diameter. The appearance of the stem-like characteristics might contribute to the increased resistance phenotype to doxorubicin that we have observed.

The activation of the Wnt/β-catenin signaling pathway was also assessed in 143B cells treated with the different fibroblasts-derived secretomes, but to see if it underlies the acquisition of stemness features, only cells treated with the $NAFs^{SCR}$-derived secretome showed a small increase in the mRNA expression of the LRP5/6 and AXIN2. Since the β-catenin translocation to the nucleus is the hallmark of the Wnt pathway activation[105], we also assessed the spatial distribution of this protein by immunofluorescence. Although we did not find evidence of β-catenin nuclear accumulation, it was observed to accumulate in the cytoplasm and not be degraded, which is the step that precedes the nuclear translocation. These data are not conclusive, and further studies are required to clarify whether the Wnt/β-catenin pathway is activated or not.

In many cancer patients, metastatic diseases occur following extended periods of disease-free survival, which remain a common cause of morbidity and mortality[27]. The appearance of tumor relapse after a prolonged time has been attributed to the ability of disseminated tumor cells entry in a long-term dormant state[137].

Dormant cells can survive in a quiescent state and remain undetected for long periods, explaining the prolonged asymptomatic residual disease[138]. This state is characterized by a temporary cell cycle arrest, where cells stop dividing and are trapped in a G0 phase. These features also contribute to a more resistant phenotype to conventional drugs because the current treatments tend to target proliferating cells[139]. Moreover, this is a reversible process, and under certain microenvironmental conditions such as the presence of growth factors, cytokines, nutrients, or chemical agents, cancer cells may escape and re-enter the cell cycle to restart proliferation[137,141].

The effects of the different fibroblasts-derived secretome were also assessed in the ability to promote the entry of 143B cells in a dormant state. Cancer cells in a continuous proliferation state exhibit constitutive ERK activation allowing G0-G1-S phase transition and cell division[142]. In this proliferation state, a high level of p38 activity functions as an inhibitory regulator of ERK and prevents cell proliferation by inducing G0-G1 arrest or triggering senescence and apoptosis. Indeed, *in vivo* studies revealed that the p38/ERK activity ratio can be an indicator of dormant cells in various cancer types, such as breast and prostate cancer, melanoma, and fibrosarcoma[138,148]. 143B cells enter into a dormant-like state after 24h of treatment with NAFs-derived secretome, as indicated by the low pERK/p-p38 ratio suggesting an adaptation step in a proliferative state as observed at the later time points of incubation (72h). At this time point, the pERK/p-p38 ratio increased to greater than 1. Interestingly, this switch from dormant to proliferation is due to increased p38 phosphorylation, whereas the ERK phosphorylated levels remain unaltered. The p38 signaling could therefore represent a potential target to unravel the mechanisms controlling the dormant-to-proliferative switch. For example, the uPAR expression and the TGF-β signaling pathway could be potential essential regulators of the entrance of 143B cells in a dormant state through their effects in the p38 phosphorylation[146,148].

Different approaches to verify the cell entry in this state should be considered, for example, a cell cycle arrest analysis [174–176], the evaluation of proliferative markers, such as Ki67 [177], and already mentioned p38 phosphorylation regulators, such as uPAR, that is described as a promoter for this protein phosphorylation as well as TGF-β.

Moreover, any regulatory factor that changes the balance of p38/ERK activity dictates whether cancer cells grow or remain dormant. The interaction between cancer cells and de ECM appears to be crucial to understanding the induction of this dormant-like phenotype.

The ECM remodeling promotes several alterations on the cancer cells phenotype, such as motility improvement, growth, and survival, affecting tumor biology and progression[148]. Additionally, cell adhesion to the ECM proteins triggers intracellular signaling pathways that can regulate cell cycle progression, migration, and differentiation, through integrins and other cell surface receptors[155]. Thus, integrin-mediated interactions between cancer cells and the ECM are critical modulators of the metastatic potential of cancer cells[156]. The binding between integrin β1 and fibronectin is described as a key factor to promote the reactivation of cancer cells from a dormant-like state to a full proliferation one. This binding promotes the alteration of the pERK/p-p38 ratio favoring ERK[144]. The highly metastatic 143B cell line already disposes high levels of integrin β1, but the activated fibroblasts' secretome exacerbates this protein expression.

The *in vitro* adhesion assay of 143B cells to fibronectin confirmed the enhanced ability of tumor cells to adhere to fibronectin when exposed to the secretome of activated fibroblasts, which can be explained by the upregulation of integrin β1. In fact, studies using a neutralizing anti-integrin β1 antibody revealed a decrease in 143B cells adhesion to fibronectin, with these effects being considerably more pronounced in cells treated with the activated fibroblasts-derived secretome.

These data suggest that cell adhesion mediated by fibronectin-binding integrin β1 might contribute to the adherence of circulating tumor cells to the pulmonary fibronectin favoring their colonization. Blockade of this interaction might be an effective strategy to decrease and/or prevent cancer cells attachment to the lung tissue, which is an important step in metastasis. Additionally, it would be also interesting to evaluate the role of integrin β1 in regulating the switch from a dormant state to active proliferation.

In sum, tumor cells, through the production and release of biomolecules, induce alterations in the lung architecture and promote the activation of fibroblasts which are

the most abundant cells in the pulmonary interstitium. The activated fibroblasts, in turn, react by orchestrating several molecular mechanisms that render tumor cells more effective at metastasizing. These findings provide evidence of mutual interaction between fibroblasts and tumor cells before the onset of lung colonization and highlight the contribution of the lung stromal microenvironment in metastatic development and cancer progression.

5. Conclusion

Based on the results obtained in this thesis, we conclude:

- Treating animals with the secretome of 143B cells promotes lung alterations similar to those induced by a primary tumor and could represent an alternative experimental approach to study the molecular mechanisms underlying the establishment of the premetastatic niche.
- Tumor cells secrete and release important biomolecules that induce structural and inflammatory changes in the lung stromal microenvironment to favor circulating tumor cells colonization and survival.
- Lung fibroblasts undergo an activation process with reciprocal effects on tumor cells, rendering them less responsive to doxorubicin, apparently through the acquisition of stem-like features.
- Tumor cells, while adapting to the secretome derived from activated fibroblasts, enter into a slow-proliferating/dormant-like state through activation of the p38 signaling pathway, followed by a progressively increased ability to proliferate.
- Treatment with the secretome of activated fibroblast increases the adhesion ability of tumor cells to fibronectin through an integrin β1-mediated pathway.

6. Future Directions

The results obtained in this work provide evidence for the active role of lung fibroblasts in the preparation of the premetastatic niche. Furthermore, it was demonstrated how the fibroblasts are educated by tumor cells in the lung stroma microenvironment and how this relevant crosstalk could lead to a more efficient metastatic process.

Based on the results obtained so far, an *in vivo* study using a neutralizing antibody against integrin β1 should be performed to evaluate if interfering with the binding integrin β1-fibronectin could prevent the formation of lung metastasis.

Proteomic analysis of the conditioned media of activated fibroblasts should be performed to identify the potential mediators that may aid the colonization of osteosarcoma cells and metastasis formation. This knowledge will contribute to understanding the molecular and cellular mechanisms that we have observed and that precede the formation of lung metastasis in osteosarcoma, as well as the identification of potential targets for therapeutic intervention.

7. References

1. Prater, S. & McKeon, B. Osteosarcoma. in (2021).
2. Zhao, X., Wu, Q., Gong, X., Liu, J. & Ma, Y. Osteosarcoma: a review of current and future therapeutic approaches. *BioMedical Engineering Online* vol. 20 (2021).
3. Fan, T. M., Roberts, R. D. & Lizardo, M. M. Understanding and Modeling Metastasis Biology to Improve Therapeutic Strategies for Combating Osteosarcoma Progression. *Frontiers in Oncology* vol. 10 (2020).
4. Rickel, K., Fang, F. & Tao, J. Molecular genetics of osteosarcoma. *Bone* **102**, 69–79 (2017).
5. Tao, J. *et al.* Notch Activation as a Driver of Osteogenic Sarcoma. *Cancer Cell* **26**, 390–401 (2014).
6. Czarnecka, A. M. *et al.* Molecular biology of osteosarcoma. *Cancers* vol. 12 1–27 (2020).
7. Gebhardt, M. C. Molecular biology of sarcomas. *Orthopedic Clinics of North America* vol. 27 421–429 (1996).
8. Corre, I., Verrecchia, F., Crenn, V., Redini, F. & Trichet, V. The Osteosarcoma Microenvironment: A Complex But Targetable Ecosystem. *Cells* vol. 9 (2020).
9. Savage, S. A. & Mirabello, L. Using epidemiology and genomics to understand osteosarcoma etiology. *Sarcoma* vol. 2011 (2011).
10. Zamborsky, R., Kokavec, M., Harsanyi, S. & Danisovic, L. Identification of Prognostic and Predictive Osteosarcoma Biomarkers. *Medical Sciences* **7**, 28 (2019).
11. Kun-Peng, Z., Chun-Lin, Z., Jian-Ping, H. & Lei, Z. A novel circulating hsa_circ_0081001 act as a potential biomarker for diagnosis and prognosis of osteosarcoma. *International Journal of Biological Sciences* **14**, 1513–1520 (2018).
12. Zhang, X. & Guan, Z. PET/CT in the diagnosis and prognosis of osteosarcoma. *Frontiers in Bioscience - Landmark* **23**, 2157–2165 (2018).
13. Yarmish, G., Klein, M. J., Landa, J., Lefkowitz, R. A. & Hwang, S. Imaging characteristics of primary osteosarcoma: Nonconventional subtypes. *Radiographics* **30**, 1653–1672 (2010).
14. Meazza, C. & Scanagatta, P. Metastatic osteosarcoma: a challenging multidisciplinary treatment. *Expert Review of Anticancer Therapy* vol. 16 543–556 (2016).
15. Martin, J. W., Squire, J. A. & Zielenska, M. The genetics of osteosarcoma. *Sarcoma* vol. 2012 (2012).
16. Sadykova, L. R. *et al.* Epidemiology and Risk Factors of Osteosarcoma. *Cancer Investigation* vol. 38 259–269 (2020).
17. Serra, M. & Hattinger, C. M. The pharmacogenomics of osteosarcoma. *Pharmacogenomics Journal* vol. 17 11–20 (2017).

18. Ta, H. T., Dass, C. R., Choong, P. F. M. & Dunstan, D. E. Osteosarcoma treatment: State of the art. *Cancer and Metastasis Reviews* vol. 28 247–263 (2009).
19. Luetke, A., Meyers, P. A., Lewis, I. & Juergens, H. Osteosarcoma treatment - Where do we stand? A state of the art review. *Cancer Treatment Reviews* vol. 40 523–532 (2014).
20. Jafari, F. *et al.* Osteosarcoma: A comprehensive review of management and treatment strategies. *Annals of Diagnostic Pathology* vol. 49 (2020).
21. Lilienthal, I. & Herold, N. Targeting molecular mechanisms underlying treatment efficacy and resistance in osteosarcoma: A review of current and future strategies. *International Journal of Molecular Sciences* vol. 21 1–56 (2020).
22. Harrison, D. J., Geller, D. S., Gill, J. D., Lewis, V. O. & Gorlick, R. Current and future therapeutic approaches for osteosarcoma. *Expert Review of Anticancer Therapy* vol. 18 39–50 (2018).
23. Vasquez, L. *et al.* Analysis of prognostic factors in high-grade osteosarcoma of the extremities in children: A 15-year single-institution experience. *Frontiers in Oncology* **6**, (2016).
24. Smrke, A. *et al.* Future Directions in the Treatment of Osteosarcoma. *Cells* vol. 10 (2021).
25. Saraf, A. J., Fenger, J. M. & Roberts, R. D. Osteosarcoma: Accelerating progress makes for a hopeful future. *Frontiers in Oncology* vol. 8 (2018).
26. Sayles, L. C. *et al.* Genome-informed targeted therapy for osteosarcoma. *Cancer Discovery* **9**, 46–63 (2019).
27. Steeg, P. S. Targeting metastasis. *Nature Reviews Cancer* vol. 16 201–218 (2016).
28. Anderson, R. L. *et al.* A framework for the development of effective anti-metastatic agents. *Nature Reviews Clinical Oncology* vol. 16 185–204 (2019).
29. Gomez-Cuadrado, L., Tracey, N., Ma, R., Qian, B. & Brunton, V. G. Mouse models of metastasis: Progress and prospects. *DMM Disease Models and Mechanisms* vol. 10 1061–1074 (2017).
30. Paget, S. *DISTRIBUTION OF SECONDARY GROWTHS IN CANCER OF THE BREAST*.
31. Peinado, H. *et al.* Pre-metastatic niches: Organ-specific homes for metastases. *Nature Reviews Cancer* vol. 17 302–317 (2017).
32. Nicolson, G. L. Organ selectivity for implantation survival and growth of b16 melanoma variant tumor lines. *Journal of the National Cancer Institute* **57**, 1199–1202 (1976).
33. Hoshino, A. *et al.* Tumour exosome integrins determine organotropic metastasis. *Nature* **527**, 329–335 (2015).
34. Bray, F. *et al.* Global cancer statistics 2018: GLOBOCAN estimates of incidence and mortality worldwide for 36 cancers in 185 countries. *CA: A Cancer Journal for Clinicians* **68**, 394–424 (2018).
35. Chaffer, C. L. & Weinberg, R. A. *A Perspective on Cancer Cell Metastasis*. http://science.sciencemag.org/.
36. Shang, C., Qiao, J. & Guo, H. The dynamic behavior of lipid droplets in the pre-metastatic niche. *Cell Death and Disease* vol. 11 (2020).
37. Zhuyan, J. *et al.* Critical steps to tumor metastasis: Alterations of tumor microenvironment and extracellular matrix in the formation of pre-metastatic and metastatic niche. *Cell and Bioscience* vol. 10 (2020).

38. Obenauf, A. C. & Massagué, J. Surviving at a Distance: Organ-Specific Metastasis. *Trends in Cancer* **1**, 76–91 (2015).
39. McDowell, S. A. C. & Quail, D. F. Immunological regulation of vascular inflammation during cancer metastasis. *Frontiers in Immunology* vol. 10 (2019).
40. Sun, T. *et al.* Anoikis resistant mediated by FASN promoted growth and metastasis of osteosarcoma. *Cell Death and Disease* **10**, (2019).
41. Guo-Sheng Zhao *et al.* High expression of ID1 facilitates metastasis in human osteosarcoma by regulating the sensitivity of anoikis via PI3K/AKT depended suppression of the intrinsic apoptotic signaling pathway. *Am J Transl Res* (2019).
42. Strauss, S. J., Ng, T., Mendoza-Naranjo, A., Whelan, J. & Sorensen, P. H. B. Understanding Micrometastatic Disease and Anoikis Resistance in Ewing Family of Tumors and Osteosarcoma . *The Oncologist* **15**, 627–635 (2010).
43. Doglioni, G., Parik, S. & Fendt, S. M. Interactions in the (pre)metastatic niche support metastasis formation. *Frontiers in Oncology* vol. 9 (2019).
44. Mazumdar, A. *et al.* Exploring the role of osteosarcoma-derived extracellular vesicles in pre-metastatic niche formation and metastasis in the 143-b xenograft mouse osteosarcoma model. *Cancers* **12**, 1–19 (2020).
45. Mazumdar, A. *et al.* Osteosarcoma-derived extracellular vesicles induce lung fibroblast reprogramming. *International Journal of Molecular Sciences* **21**, 1–20 (2020).
46. Mina, L. A. & Sledge, G. W. Rethinking the metastatic cascade as a therapeutic target. *Nature Reviews Clinical Oncology* **8**, 325–332 (2011).
47. Majidpoor, J. & Mortezaee, K. Steps in metastasis: an updated review. *Medical Oncology* vol. 38 (2021).
48. Liu, Y. & Cao, X. Organotropic metastasis: Role of tumor exosomes. *Cell Research* vol. 26 149–150 (2016).
49. Gao, Y. *et al.* Metastasis Organotropism: Redefining the Congenial Soil. *Developmental Cell* **49**, 375–391 (2019).
50. Urabe, F., Patil, K., Ramm, G. A., Ochiya, T. & Soekmadji, C. Extracellular vesicles in the development of organ-specific metastasis. *Journal of Extracellular Vesicles* **10**, (2021).
51. Chicón-Bosch, M. & Tirado, O. M. Exosomes in Bone Sarcomas: Key Players in Metastasis. *Cells* vol. 9 (2020).
52. Hinshaw, D. C. & Shevde, L. A. The tumor microenvironment innately modulates cancer progression. *Cancer Research* vol. 79 4557–4567 (2019).
53. Baghban, R. *et al.* Tumor microenvironment complexity and therapeutic implications at a glance. *Cell Communication and Signaling* **18**, 1–19 (2020).
54. Wortzel, I., Dror, S., Kenific, C. M. & Lyden, D. Exosome-Mediated Metastasis: Communication from a Distance. *Developmental Cell* vol. 49 347–360 (2019).
55. Zhou, Y., Han, M. & Gao, J. Prognosis and targeting of pre-metastatic niche. *Journal of Controlled Release* vol. 325 223–234 (2020).
56. Weidle, U. H., Birzele, F., Kollmorgen, G. & Rüger, R. The multiple roles of exosomes in metastasis. *Cancer Genomics and Proteomics* vol. 14 1–16 (2017).
57. Boukouris, S. & Mathivanan, S. Exosomes in bodily fluids are a highly stable resource of disease biomarkers. *Proteomics - Clinical Applications* vol. 9 358–367 (2015).

58. Guo, Y. *et al.* Effects of exosomes on pre-metastatic niche formation in tumors. *Molecular Cancer* vol. 18 (2019).
59. Saha, K., Banerjee, A., Jash, D. & Saha, D. Osteosarcoma relapse as pleural metastasis. *South Asian Journal of Cancer* **2**, 56 (2013).
60. Wang, Y., Ren, X., Yuan, Y. & Yuan, B.-S. Downregulated lncRNA GAS5 and Upregulated miR-21 Lead to Epithelial–Mesenchymal Transition and Lung Metastasis of Osteosarcomas. *Frontiers in Cell and Developmental Biology* **9**, (2021).
61. Azevedo, A. S., Follain, G., Patthabhiraman, S., Harlepp, S. & Goetz, J. G. Metastasis of circulating tumor cells: Favorable soil or suitable biomechanics, or both? *Cell Adhesion and Migration* vol. 9 345–356 (2015).
62. Mo, Z. *et al.* Extracellular vesicle-associated organotropic metastasis. *Cell Proliferation* vol. 54 (2021).
63. Liu, Y. *et al.* Tumor Exosomal RNAs Promote Lung Pre-metastatic Niche Formation by Activating Alveolar Epithelial TLR3 to Recruit Neutrophils. *Cancer Cell* **30**, 243–256 (2016).
64. Vu, L. T. *et al.* Tumor-secreted extracellular vesicles promote the activation of cancer-associated fibroblasts via the transfer of microRNA-125b. *Journal of Extracellular Vesicles* **8**, (2019).
65. Goulet, C. R. *et al.* Exosomes induce fibroblast differentiation into cancer-associated fibroblasts through TGFb signaling. *Molecular Cancer Research* **16**, 1196–1204 (2018).
66. Avagliano, A. *et al.* Metabolic Reprogramming of Cancer Associated Fibroblasts: The Slavery of Stromal Fibroblasts. *BioMed Research International* vol. 2018 (2018).
67. Santi, A., Kugeratski, F. G. & Zanivan, S. Cancer Associated Fibroblasts: The Architects of Stroma Remodeling. *Proteomics* vol. 18 (2018).
68. Arcucci, A., Ruocco, M. R., Granato, G., Sacco, A. M. & Montagnani, S. Cancer: An Oxidative Crosstalk between Solid Tumor Cells and Cancer Associated Fibroblasts. *BioMed Research International* **2016**, (2016).
69. Tao, L., Huang, G., Song, H., Chen, Y. & Chen, L. Cancer associated fibroblasts: An essential role in the tumor microenvironment (review). *Oncology Letters* vol. 14 2611–2620 (2017).
70. Wu, X. *et al.* Extracellular vesicle packaged LMP1-activated fibroblasts promote tumor progression via autophagy and stroma-tumor metabolism coupling. *Cancer Letters* **478**, 93–106 (2020).
71. Sahai, E. *et al.* A framework for advancing our understanding of cancer-associated fibroblasts. *Nature Reviews Cancer* vol. 20 174–186 (2020).
72. Liu, T., Zhou, L., Li, D., Andl, T. & Zhang, Y. Cancer-associated fibroblasts build and secure the tumor microenvironment. *Frontiers in Cell and Developmental Biology* vol. 7 (2019).
73. Shoucair, I., Mello, F. W., Jabalee, J., Maleki, S. & Garnis, C. The role of cancer-associated fibroblasts and extracellular vesicles in tumorigenesis. *International Journal of Molecular Sciences* vol. 21 1–37 (2020).
74. Webber, J. P. *et al.* Differentiation of tumour-promoting stromal myofibroblasts by cancer exosomes. *Oncogene* **34**, 319–333 (2015).

75. Shiga, K. *et al.* Cancer-associated fibroblasts: Their characteristics and their roles in tumor growth. *Cancers* vol. 7 2443–2458 (2015).
76. Wang, Z. *et al.* Metastasis-associated fibroblasts: an emerging target for metastatic cancer. *Biomarker Research* vol. 9 (2021).
77. Pein, M. *et al.* Metastasis-initiating cells induce and exploit a fibroblast niche to fuel malignant colonization of the lungs. *Nature Communications* **11**, (2020).
78. Duda, D. G. *et al.* Malignant cells facilitate lung metastasis by bringing their own soil. *Proceedings of the National Academy of Sciences of the United States of America* **107**, 21677–21682 (2010).
79. Fang, T. *et al.* Tumor-derived exosomal miR-1247-3p induces cancer-associated fibroblast activation to foster lung metastasis of liver cancer. *Nature Communications* **9**, (2018).
80. Kong, J. *et al.* Extracellular vesicles of carcinoma-associated fibroblasts creates a pre-metastatic niche in the lung through activating fibroblasts. *Molecular Cancer* **18**, (2019).
81. Webber, J., Steadman, R., Mason, M. D., Tabi, Z. & Clayton, A. Cancer exosomes trigger fibroblast to myofibroblast differentiation. *Cancer Research* **70**, 9621–9630 (2010).
82. Gong, L. *et al.* Exosomal miR-675 from metastatic osteosarcoma promotes cell migration and invasion by targeting CALN1. *Biochemical and Biophysical Research Communications* **500**, 170–176 (2018).
83. Chowdhury, R. *et al. Cancer exosomes trigger mesenchymal stem cell differentiation into pro-angiogenic and pro-invasive myofibroblasts*. vol. 6 www.impactjournals.com/oncotarget.
84. Kaplan, R. N. *et al.* VEGFR1-positive haematopoietic bone marrow progenitors initiate the pre-metastatic niche. *Nature* **438**, 820–827 (2005).
85. LeBleu, V. S. & Kalluri, R. A peek into cancer-associated fibroblasts: Origins, functions and translational impact. *DMM Disease Models and Mechanisms* **11**, (2018).
86. Batlle, E. & Clevers, H. Cancer stem cells revisited. *Nature Medicine* **23**, 1124–1134 (2017).
87. Malanchi, I. *et al.* Interactions between cancer stem cells and their niche govern metastatic colonization. *Nature* **481**, 85–91 (2012).
88. Costa, A. *et al.* Fibroblast Heterogeneity and Immunosuppressive Environment in Human Breast Cancer. *Cancer Cell* **33**, 463-479.e10 (2018).
89. Kalluri, R. The biology and function of fibroblasts in cancer. *Nature Reviews Cancer* vol. 16 582–598 (2016).
90. Orimo, A. *et al.* Stromal fibroblasts present in invasive human breast carcinomas promote tumor growth and angiogenesis through elevated SDF-1/CXCL12 secretion. *Cell* **121**, 335–348 (2005).
91. Kwa, M. Q., Herum, K. M. & Brakebusch, C. Cancer-associated fibroblasts: how do they contribute to metastasis? *Clinical and Experimental Metastasis* vol. 36 71–86 (2019).
92. Toh, T. B., Lim, J. J. & Chow, E. K. H. Epigenetics in cancer stem cells. *Molecular Cancer* **16**, 1–20 (2017).

93. Cao, J. *et al.* Cancer stem cells and strategies for targeted drug delivery. *Drug Delivery and Translational Research* **11**, 1779–1805 (2021).
94. Yan, G. N., Lv, Y. F. & Guo, Q. N. Advances in osteosarcoma stem cell research and opportunities for novel therapeutic targets. *Cancer Letters* **370**, 268–274 (2016).
95. Brown, H. K., Tellez-Gabriel, M. & Heymann, D. Cancer stem cells in osteosarcoma. *Cancer Letters* **386**, 189–195 (2017).
96. Tirino, V., Desiderio, V., Paino, F., Papaccio, G. & de Rosa, M. Methods for cancer stem cell detection and isolation. *Methods in Molecular Biology* **879**, 513–529 (2012).
97. Yang, M., Yan, M., Zhang, R., Li, J. & Luo, Z. Side population cells isolated from human osteosarcoma are enriched with tumor-initiating cells. *Cancer Science* **102**, 1774–1781 (2011).
98. Martins-Neves, S. R. *et al.* Therapeutic implications of an enriched cancer stem-like cell population in a human osteosarcoma cell line. *BMC Cancer* **12**, (2012).
99. HONOKI, K. *et al.* Possible involvement of stem-like populations with elevated ALDH1 in sarcomas for chemotherapeutic drug resistance. *ONCOLOGY REPORTS* **24**, 501–505 (2010).
100. Wang, L., Park, P., Zhang, H., la Marca, F. & Lin, C. Y. Prospective identification of tumorigenic osteosarcoma cancer stem cells in OS99-1 cells based on high aldehyde dehydrogenase activity. *International Journal of Cancer* **128**, 294–303 (2011).
101. Greco, N. *et al.* ALDH Activity Correlates with Metastatic Potential in Primary Sarcomas of Bone. *J Cancer Ther* 331–338 (2014) doi:10.4236/jct.2014.54040.
102. Martins-Neves, S. R. *et al.* Osteosarcoma Stem Cells Have Active Wnt/β-catenin and Overexpress SOX2 and KLF4. *Journal of Cellular Physiology* **231**, 876–886 (2016).
103. Lv, F. J., Tuan, R. S., Cheung, K. M. C. & Leung, V. Y. L. Concise review: The surface markers and identity of human mesenchymal stem cells. *Stem Cells* **32**, 1408–1419 (2014).
104. Mutsaers, A. J. & Walkley, C. R. Cells of origin in osteosarcoma: Mesenchymal stem cells or osteoblast committed cells? *Bone* **62**, 56–63 (2014).
105. Singla, A. *et al.* Wnt signaling in osteosarcoma. *Advances in Experimental Medicine and Biology* **1258**, 125–139 (2020).
106. Zhang, H. *et al.* Transforming growth factor β1 signal is crucial for dedifferentiation of cancer cells to cancer stem cells in osteosarcoma. *Stem Cells* **31**, 433–446 (2013).
107. Manuscript, A. TGFβ in Cancer.pdf. **134**, 215–230 (2012).
108. Karamboulas, C. & Ailles, L. Developmental signaling pathways in cancer stem cells of solid tumors. *Biochimica et Biophysica Acta - General Subjects* **1830**, 2481–2495 (2013).
109. Nandy, S. B. & Lakshmanaswamy, R. *Cancer Stem Cells and Metastasis*. *Progress in Molecular Biology and Translational Science* vol. 151 (Elsevier Inc., 2017).
110. Liu, S. *et al.* Hedgehog signaling and Bmi-1 regulate self-renewal of normal and malignant human mammary stem cells. *Cancer Research* **66**, 6063–6071 (2006).

111. Rizzo, P. *et al.* Rational targeting of Notch signaling in cancer. *Oncogene* **27**, 5124–5131 (2008).
112. Ling, L., Nurcombe, V. & Cool, S. M. Wnt signaling controls the fate of mesenchymal stem cells. *Gene* **433**, 1–7 (2009).
113. Basu-Roy, U. *et al.* Sox2 maintains self renewal of tumor-initiating cells in osteosarcomas. *Oncogene* **31**, 2270–2282 (2012).
114. Babaei, G., Aziz, S. G. G. & Jaghi, N. Z. Z. EMT, cancer stem cells and autophagy; The three main axes of metastasis. *Biomedicine and Pharmacotherapy* **133**, 110909 (2021).
115. Joyce, J. A. & Pollard, J. W. Microenvironmental regulation of metastasis. *Nature Reviews Cancer* **9**, 239–252 (2009).
116. Lin, C. H., Ji, T., Chen, C. F. & Hoang, B. H. Wnt signaling in osteosarcoma. *Advances in Experimental Medicine and Biology* **804**, 33–45 (2014).
117. Gaston-Massuet, C. *et al.* Increased Wingless (Wnt) signaling in pituitary progenitor/stem cells gives rise to pituitary tumors in mice and humans. *Proceedings of the National Academy of Sciences of the United States of America* **108**, 11482–11487 (2011).
118. Yu, Z., Pestell, T. G., Lisanti, M. P. & Pestell, R. G. Cancer stem cells. *International Journal of Biochemistry and Cell Biology* **44**, 2144–2151 (2012).
119. Martins-Neves, S. R. *et al.* IWR-1, a tankyrase inhibitor, attenuates Wnt/β-catenin signaling in cancer stem-like cells and inhibits in vivo the growth of a subcutaneous human osteosarcoma xenograft. *Cancer Letters* **414**, 1–15 (2018).
120. Kubota, T., Michigami, T. & Ozono, K. Wnt signaling in bone. *Clinical Pediatric Endocrinology* **19**, 49–56 (2010).
121. Hosseini, F. *et al.* Targeting Wnt/β-catenin signaling by microRNAs as a therapeutic approach in chemoresistant osteosarcoma. *Biochemical Pharmacology* **193**, 114758 (2021).
122. McQueen, P. *et al.* The Wnt signaling pathway: Implications for therapy in osteosarcoma. *Expert Review of Anticancer Therapy* **11**, 1223–1232 (2011).
123. Ahn, V. E. *et al.* Structural basis of Wnt signaling inhibition by Dickkopf binding to LRP5/6. *Developmental Cell* **21**, 862–873 (2011).
124. Goldstein, S. D., Trucco, M., Guzman, W. B., Hayashi, M. & Loeb, D. M. A monoclonal antibody against the Wnt signaling inhibitor dickkopf-1 inhibits osteosarcoma metastasis in a preclinical model. *Oncotarget* **7**, 21114–21123 (2016).
125. Kimura, H. *et al.* CKAP4 is a Dickkopf1 receptor and is involved in tumor progression. *Journal of Clinical Investigation* **126**, 2689–2705 (2016).
126. Malladi, S. *et al.* Metastatic Latency and Immune Evasion through Autocrine Inhibition of WNT. *Cell* **165**, 45–60 (2016).
127. Marchandet, L. *et al.* Mechanisms of resistance to conventional therapies for osteosarcoma. *Cancers* **13**, 1–24 (2021).
128. He, H., Ni, J. & Huang, J. Molecular mechanisms of chemoresistance in osteosarcoma (review). *Oncology Letters* **7**, 1352–1362 (2014).
129. Garcia-Mayea, Y., Mir, C., Masson, F., Paciucci, R. & LLeonart, M. E. Insights into new mechanisms and models of cancer stem cell multidrug resistance. *Seminars in Cancer Biology* **60**, 166–180 (2020).

130. Najafi, M., Mortezaee, K. & Majidpoor, J. Cancer stem cell (CSC) resistance drivers. *Life Sciences* **234**, (2019).
131. Prager, B. C., Xie, Q., Bao, S. & Rich, J. N. Cancer Stem Cells: The Architects of the Tumor Ecosystem. *Cell Stem Cell* **24**, 41–53 (2019).
132. Dianat-Moghadam, H. *et al.* Cancer stem cells-emanated therapy resistance: Implications for liposomal drug delivery systems. *Journal of Controlled Release* **288**, 62–83 (2018).
133. Liu, B., Ma, W., Jha, R. K. & Gurung, K. Cancer stem cells in osteosarcoma: Recent progress and perspective. *Acta Oncologica* **50**, 1142–1150 (2011).
134. Izadpanah, S. *et al.* Prospects for the involvement of cancer stem cells in the pathogenesis of osteosarcoma. *Journal of Cellular Physiology* **235**, 4167–4182 (2020).
135. Reina-Campos, M., Shelton, P. M., Diaz-Meco, M. T. & Moscat, J. Metabolic reprogramming of the tumor microenvironment by p62 and its partners. *Biochimica et Biophysica Acta - Reviews on Cancer* **1870**, 88–95 (2018).
136. Bocci, F. *et al.* Toward understanding cancer stem cell heterogeneity in the tumor microenvironment. *Proceedings of the National Academy of Sciences of the United States of America* **116**, 148–157 (2019).
137. Butturini, E., de Prati, A. C., Boriero, D. & Mariotto, S. Tumor dormancy and interplay with hypoxic tumor microenvironment. *International Journal of Molecular Sciences* **20**, (2019).
138. Aguirre-ghiso, J. A. Models , mechanisms and clinical evidence for cancer dormancy. **7**, 834–847 (2007).
139. Zhu, L., McManus, M. M. & Hughes, D. P. M. Understanding the biology of bone sarcoma from early initiating events through late events in metastasis and disease progression. *Frontiers in Oncology* **3 SEP**, 1–17 (2013).
140. Recasens, A. & Munoz, L. Targeting Cancer Cell Dormancy. *Trends in Pharmacological Sciences* **40**, 128–141 (2019).
141. Gomis, R. R. & Gawrzak, S. Tumor cell dormancy. *Molecular Oncology* **11**, 62–78 (2017).
142. Chambard, J. C., Lefloch, R., Pouysségur, J. & Lenormand, P. ERK implication in cell cycle regulation. *Biochimica et Biophysica Acta - Molecular Cell Research* **1773**, 1299–1310 (2007).
143. Aguirre-Ghiso, J. A., Estrada, Y., Liu, D. & Ossowski, L. ERKMAPK activity as a determinant of tumor growth and dormancy; regulation by p38SAPK. *Cancer Research* **63**, 1684–1695 (2003).
144. Park, S. Y. & Nam, J. S. The force awakens: metastatic dormant cancer cells. *Experimental and Molecular Medicine* **52**, 569–581 (2020).
145. Allgayer, H. & Aguirre-Ghiso, J. A. The urokinase receptor (u-PAR) - A link between tumor cell dormancy and minimal residual disease in bone marrow? *Apmis* **116**, 602–614 (2008).
146. Koul, H. K., Pal, M. & Koul, S. Role of p38 MAP Kinase Signal Transduction in Solid Tumors. *Genes and Cancer* **4**, 342–359 (2013).
147. Bragado, P. *et al.* TGF-β2 dictates disseminated tumour cell fate in target organs through TGF-β-RIII and p38α/β signalling. *Nature Cell Biology* **15**, 1351–1361 (2013).

148. Parker, A. L. & Cox, T. R. The Role of the ECM in Lung Cancer Dormancy and Outgrowth. *Frontiers in Oncology* **10**, (2020).
149. Puig, M. *et al.* Matrix stiffening and β1 integrin drive subtype-specific fibroblast accumulation in lung cancer. *Molecular Cancer Research* **13**, 161–173 (2015).
150. Wang, M. *et al.* Thrombospondin enhances RANKL-dependent osteoclastogenesis and facilitates lung cancer bone metastasis. *Biochemical Pharmacology* **166**, 23–32 (2019).
151. Oskarsson, T. *et al.* Breast cancer cells produce tenascin C as a metastatic niche component to colonize the lungs. *Nat Med* **17(7)**, 867–874 (2014).
152. del Pozo Martin, Y. *et al.* Mesenchymal Cancer Cell-Stroma Crosstalk Promotes Niche Activation, Epithelial Reversion, and Metastatic Colonization. *Cell Reports* **13**, 2456–2469 (2015).
153. Chaudhri, V. K. *et al.* Metabolic alterations in lung cancer-associated fibroblasts correlated with increased glycolytic metabolism of the tumor. *Molecular Cancer Research* **11**, 579–592 (2013).
154. Barkan, D., Green, J. E. & Chambers, A. F. Extracellular matrix: A gatekeeper in the transition from dormancy to metastatic growth. *European Journal of Cancer* **46**, 1181–1188 (2010).
155. White, D. E., Rayment, J. H. & Muller, W. J. Addressing the role of cell adhesion in tumor cell dormancy. *Cell Cycle* **5**, 1756–1759 (2006).
156. Barkan, D. & Chambers, A. F. β1-integrin: A potential therapeutic target in the battle against cancer recurrence. *Clinical Cancer Research* **17**, 7219–7223 (2011).
157. Bratt-Leal, A. M., Carpenedo, R. L., Ungrin, M. D., Zandstra, P. W. & McDevitt, T. C. Incorporation of biomaterials in multicellular aggregates modulates pluripotent stem cell differentiation. *Biomaterials* **32**, 48–56 (2011).
158. Silva, A. *et al.* Calcium modulation, anti-oxidant and anti-inflammatory effect of skin allergens targeting the Nrf2 signaling pathway in alzheimer's disease cellular models. *International Journal of Molecular Sciences* **21**, 1–22 (2020).
159. Aires, I. D. *et al.* Exosomes derived from microglia exposed to elevated pressure amplify the neuroinflammatory response in retinal cells. *GLIA* **68**, 2705–2724 (2020).
160. Neves, B. M. *et al.* Differential roles of PI3-Kinase, MAPKs and NF-κB on the manipulation of dendritic cell Th1/Th2 cytokine/chemokine polarizing profile. *Molecular Immunology* **46**, 2481–2492 (2009).
161. Moura, L. I. F. *et al.* Neurotensin modulates the migratory and inflammatory response of macrophages under hyperglycemic conditions. *BioMed Research International* **2013**, (2013).
162. Bailey-Downs, L. C. *et al.* Aging exacerbates obesity-induced oxidative stress and inflammation in perivascular adipose tissue in mice: a paracrine mechanism contributing to vascular redox dysregulation and inflammation. *The journals of gerontology. Series A, Biological sciences and medical sciences* **68**, 780–792 (2013).
163. Paiva-Oliveira, D. I., Martins-Neves, S. R., Abrunhosa, A. J., Fontes-Ribeiro, C. & Gomes, C. M. F. Therapeutic potential of the metabolic modulator Metformin

on osteosarcoma cancer stem-like cells. *Cancer Chemotherapy and Pharmacology* **81**, 49–63 (2018).

164. Aguirre-Ghiso, J. A., Liu, D., Mignatti, A., Kovalski, K. & Ossowski, L. Urokinase receptor and fibronectin regulate the ERKMAPK to p38MAPK activity ratios that determine carcinoma cell proliferation or dormancy in vivo. *Molecular Biology of the Cell* **12**, 863–879 (2001).
165. Liu, T. *et al.* CRISPR-Cas9-Mediated Silencing of CD44 in Human Highly Metastatic Osteosarcoma Cells. *Cellular Physiology and Biochemistry* **46**, 1218–1230 (2018).
166. Aguado, B. A. *et al.* Extracellular matrix mediators of metastatic cell colonization characterized using scaffold mimics of the pre-metastatic niche. *Acta Biomaterialia* **33**, 13–24 (2016).
167. Kidera, Y. *et al.* Reduction of lung metastasis, cell invasion, and adhesion in mouse melanoma by statin-induced blockade of the Rho/Rho-associated coiled-coil-containing protein kinase pathway. *Journal of Experimental and Clinical Cancer Research* **29**, 1–11 (2010).
168. Sliogeryte, K. & Gavara, N. Vimentin Plays a Crucial Role in Fibroblast Ageing by Regulating Biophysical Properties and Cell Migration. *Cells* **8**, (2019).
169. Rahimi, F., Hsu, K., Endoh, Y. & Geczy, C. L. FGF-2, IL-1β and TGF-β regulate fibroblast expression of S100A8. *FEBS Journal* **272**, 2811–2827 (2005).
170. Itoh, H. *et al.* TET2-dependent IL-6 induction mediated by the tumor microenvironment promotes tumor metastasis in osteosarcoma. *Oncogene* **37**, 2903–2920 (2018).
171. Gu, S. & Feng, X. H. TGF-β signaling in cancer. *Acta Biochimica et Biophysica Sinica* **50**, 941–949 (2018).
172. Xie, F., Ling, L., van Dam, H., Zhou, F. & Zhang, L. TGF-β signaling in cancer metastasis. *Acta Biochimica et Biophysica Sinica* **50**, 121–132 (2018).
173. Martins-Neves, S. R. *et al.* Chemotherapy induces stemness in osteosarcoma cells through activation of Wnt/β-catenin signaling. *Cancer Letters* **370**, 286–295 (2016).
174. Xu, S. *et al.* 6-Gingerol induces cell-cycle G1-phase arrest through AKT–GSK 3β–cyclin D1 pathway in renal-cell carcinoma. *Cancer Chemotherapy and Pharmacology* **85**, 379–390 (2020).
175. Han, Y. H., Mun, J. G., Jeon, H. D. & Kee, J. Y. Betulin inhibits lung metastasis by inducing cell cycle arrest, autophagy, and apoptosis of metastatic colorectal cancer cells. *Nutrients* **12**, (2020).
176. Zheng, J. *et al.* Novel ferrocene derivatives induce G0/G1 cell cycle arrest and apoptosis through the mitochondrial pathway in human hepatocellular carcinoma. *International Journal of Molecular Sciences* **22**, 1–13 (2021).
177. Sales Gil, R. & Vagnarelli, P. Ki-67: More Hidden behind a 'Classic Proliferation Marker.' *Trends in Biochemical Sciences* **43**, 747–748 (2018).